

Dual-Polarized IRS-Assisted MIMO Network

Muteen Munawar and Kyungchun Lee, *Senior Member, IEEE*

Abstract

This study considers a dual-polarized intelligent reflecting surface (DP-IRS)-assisted multiple-input multiple-output (MIMO) single-user wireless communication system. The transmitter and receiver are equipped with DP antennas, and each antenna features a separate phase shifter for each polarization. We attempt to maximize the system's spectral efficiency (SE) by optimizing the operations of the reflecting elements at the DP-IRS, precoder/combiner at the transmitter/receiver, and vertical/horizontal phase shifters at the DP antennas. To address this problem, we propose a three-step alternating optimization (AO) algorithm based on the semi-definite relaxation method. Next, we consider asymptotically low/high signal-to-noise ratio (SNR) regimes and propose low-complexity algorithms. In particular, for the low-SNR regime, we derive computationally low-cost closed-form solutions. According to the obtained numerical results, the proposed algorithm outperforms the various benchmark schemes. Specifically, our main algorithm exhibits a 65.6 % increase in the SE performance compared to random operations. In addition, we compare the SE performance of DP-IRS with that of simple IRS (S-IRS). For $N = 50$, DP-IRS achieves 24.8 %, 28.2 %, and 30.3 % improvements in SE for 4×4 , 8×8 , and 16×16 MIMO, respectively, compared to S-IRS.

Index Terms

Intelligent reflecting surface, dual polarization, multiple-input multiple-output, alternating optimization.

I. INTRODUCTION

An intelligent reflecting surface (IRS) is a metasurface [1] with several reflecting elements of the passive nature [2]. By applying a bias voltage, we can alter the material characteristics of these elements [3], resulting in a change in the amplitudes and phases of the impinging signals. Owing

This work was supported in part by the Basic Science Research Program through the National Research Foundation of Korea (NRF) funded by the Ministry of Education under Grant NRF-2019R1A6A1A03032119 and in part by the NRF Grant funded by the Korean Government (MSIT) under Grant NRF-2022R1A2C1006566. (Corresponding author: Kyungchun Lee.)

M. Munawar and K. Lee are with the Department of Electrical and Information Engineering and the Research Center for Electrical and Information Technology, Seoul National University of Science and Technology, Seoul 01811, Republic of Korea (e-mail: muteen@seoultech.ac.kr, kcllee@seoultech.ac.kr).

to its real-time configuration [4], IRS is considered a potential candidate for next-generation wireless communication systems [5]. In the literature, the IRS has been used to improve the signal-to-noise ratio (SNR) [3], [6], [7], increase security [8]–[12], reduce interference [6], [13], [14], transfer power [15], [16], and reflect modulation [17]. In addition, fast channel estimation methods and low-complexity beamforming schemes for IRS have been studied in the literature [18]–[21].

The introduction of dual polarization (DP) in metasurfaces can further increase their capabilities with polarization diversity (PD) [22], [23], polarization multiplexing (PM) [24], and polarization modulation [25]. Although modern communication systems operate with dual-polarized waves, to the best of our knowledge, only a few studies exist on the application of DP-IRS. For instance, in [26], the authors adopted DP-IRS for PM, to reduce the interference problem in the system. Furthermore, in [27], the authors exploited the orthogonal property of DP-IRS to transmit two data streams by modulating the data directly on the reflecting elements. Based on the inherent properties of dual polarization, there is a need to further explore the potential benefits of DP-IRS.

Here, we consider a DP-IRS-assisted narrow-band multiple-input multiple-out (MIMO) wireless communication network, where the transmitter, i.e., access point (AP), and receiver, i.e., user, are equipped with multiple DP antennas [28]. Each DP antenna is equipped with a single RF chain and a phase shifter for each polarization [29]. We attempt to maximize the spectral efficiency of the DP-IRS-assisted MIMO network by optimizing the operation of the DP-IRS. Only a few studies exist on capacity maximization for IRS, which are limited to simple IRS (S-IRS)-assisted MIMO networks [30]. For example, in [31], the authors optimized the reflecting elements of the S-IRS, where the transmitter and receiver were equipped with single polarized antennas. Similarly, in [32], the authors considered an S-IRS-assisted MIMO network and exploited millimeter-wave channel characteristics to devise low-complexity beamforming methods and maximize the achievable rate. However, to simplify the problem in [32], the authors assumed a weak AP-user channel and only considered the AP-IRS-user link in the optimization problem. In our proposed technique, we consider DP-IRS and assume both direct and reflected links in the problem. Our main contributions are summarized as follows.

- We study the DP-IRS-assisted MIMO wireless network and formulate a capacity maximization problem, which is non-convex. To solve this problem, we decompose the problem into several sub-problems and propose a semi-definite relaxation (SDR)-based alternating opti-

mization (AO) algorithm. The algorithm works by optimizing the operation of the reflecting elements at the DP-IRS, precoder/combiner matrices at the AP/user, and vertical/horizontal phase shifters at DP antennas alternatively, until the spectral efficiency converges. The algorithm and problem formulations are designed such that the objective value stays non-decreasing and is guaranteed to converge.

- Next, we consider two special cases: 1) low-SNR regime and/or line of sight (LoS) scenario and 2) high-SNR regime and rich scattered environment. Case 1 occurs when the user is in the low-SNR regime and/or the dominant channel between the AP and the user is LoS. The LoS channel occurs when the IRS is mounted in the AP's line of sight. Similarly, high-SNR and rich-scattered environments favor Case 2. We propose two low-complexity AO algorithms to maximize the spectral efficiency for these two special cases. Specifically, for Case 1, we derive closed-form solutions.
- Finally, we provide an extensive numerical analysis of the system to demonstrate the proposed algorithms' convergence behaviors and SE performances.

The remainder of this paper is organized as follows. Section II discusses the system model and formulates the capacity-maximization problem. The proposed algorithms are presented in Sections III and IV. In Section V, we numerically evaluate the performance of the proposed algorithms and compare them with benchmark schemes. Finally, Section VI concludes the paper.

Notations: Scalars are denoted by italic letters, whereas vectors and matrices are denoted by bold-face lower- and upper-case letters, respectively. The subscripts/superscripts v and h denote vertical and horizontal polarizations, respectively. For a complex-valued vector \mathbf{v} of length K , $(\mathbf{v})^T$ denotes the transpose, \mathbf{v}_k denotes the k th element of \mathbf{v} , \mathbf{v}^* denotes the complex conjugate of each element, \mathbf{v}^H denotes the conjugate transpose, $\|\mathbf{v}\|$ denotes the Euclidean norm, $\text{diag}(\mathbf{v})$ denotes a diagonal matrix with each diagonal element being the corresponding element in \mathbf{v} , $\text{arg}(\mathbf{v})$ denotes a vector with each element being the phase of the corresponding element in \mathbf{v} , $\text{logsum}(\mathbf{v})$ means $\sum_{k=1}^K \log(\mathbf{v}_k)$, $\text{sum}(\mathbf{v})$ means $\sum_{k=1}^K (\mathbf{v}_k)$, and $\text{GM}(\mathbf{v})$ represents the geometric mean. For a complex-valued matrix \mathbf{M} , $\text{rank}(\mathbf{M})$ denotes the rank, $\mathbf{M}_{(n,m)}$ denotes the n th row and m th column entry, \mathbf{M}^\dagger denotes the pseudoinverse, $\|\mathbf{M}\|$ denotes the Frobenius norm, $\mathbf{M}_{\succeq 0}$ denotes positive semi-definite, $\text{trace}(\mathbf{M})$ denotes trace, $\mathbf{M} \circ \mathbf{M}$ denotes the Hadamard product, and $\det(\mathbf{M})$ denotes the determinant. For a complex-valued square matrix \mathbf{A} , $\mathbf{I}_{\mathbf{A}}$ denotes an identity matrix of size \mathbf{A} . The notation $(\cdot)^*$ denotes the complex conjugate of a complex number.

II. SYSTEM MODEL

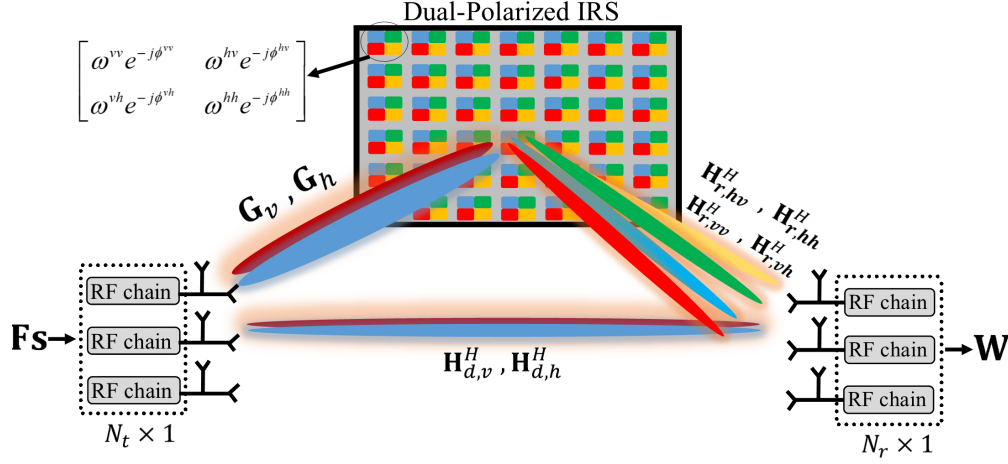


Fig. 1. System model.

We consider a DP-IRS-aided MIMO wireless communication network, as illustrated in Fig. 1. The AP and user are equipped with N_t and N_r DP antennas, respectively, and each DP antenna is connected to a single RF chain but with separate phase shifters for each polarization [28], [29]. DP-IRS comprises N passive reflecting elements, and the operation of each element can be defined by the following transformation matrix [26]:

$$\Psi = \begin{bmatrix} \omega^{vv} e^{-j\phi^{vv}} & \omega^{hv} e^{-j\phi^{hv}} \\ \omega^{vh} e^{-j\phi^{vh}} & \omega^{hh} e^{-j\phi^{hh}} \end{bmatrix}, \quad (1)$$

where $\omega^{pq} \in [0, 1]$ and $\phi^{pq} \in [0, 2\pi)$ represent the amplitude and phase changes of the reflected signal from polarization p to q , respectively, and $p, q \in \{v, h\}$. The transformation matrix (1) elucidates that the DP-IRS, in addition to possessing the ability for phase and amplitude control, which is also a feature of S-IRS, can effectively execute polarization beam splitting, independent control of incident polarization, and polarization conversion. The attributes and characteristics of these DP-IRSs have been thoroughly investigated in the domains of antennas and electromagnetic theory, as evidenced by the works of [33]–[35]. Moreover, their potential has been exploited in the context of non-orthogonal multiple access networks [26].

The received signal at the user is a linear superposition of two signals originating from the AP and DP-IRS, respectively. Considering only a single antenna and a solitary reflecting element

at the AP/user and DP-IRS, respectively, the aggregate noise-free signal received by the user is expressed as

$$\begin{aligned} \begin{bmatrix} y^v \\ y^h \end{bmatrix} &= \begin{pmatrix} e^{-j\gamma^v} & 0 \\ 0 & e^{-j\gamma^h} \end{pmatrix} \left[\left\{ \begin{pmatrix} (h_r^{vv})^* & (h_r^{hv})^* \\ (h_r^{vh})^* & (h_r^{hh})^* \end{pmatrix} \right. \right. \\ &\quad \left. \left. \circ \underbrace{\begin{pmatrix} \omega^{vv} e^{-j\phi^{vv}} & \omega^{hv} e^{-j\phi^{hv}} \\ \omega^{vh} e^{-j\phi^{vh}} & \omega^{hh} e^{-j\phi^{hh}} \end{pmatrix}}_{\Psi} \circ \begin{pmatrix} g^{vv} & g^{hv} \\ g^{vh} & g^{hh} \end{pmatrix} \right. \\ &\quad \left. \left. + \begin{pmatrix} (h_d^v)^* & 0 \\ 0 & (h_d^h)^* \end{pmatrix} \right\}^T \begin{pmatrix} \sqrt{\frac{P_t}{2}} e^{-j\theta^v} & 0 \\ 0 & \sqrt{\frac{P_t}{2}} e^{-j\theta^h} \end{pmatrix} \right]^T x, \end{aligned} \quad (2)$$

where y^v , y^h , $(h_r)^*$, $(h_d)^*$, g , and x denote the received vertical polarized signal, received horizontal polarized signal, IRS-user channel, AP-user channel, AP-IRS channel, and transmitted symbol, respectively. The matrices $\text{diag}\left(\frac{P_t}{2}e^{-j\theta^v}, \frac{P_t}{2}e^{-j\theta^h}\right)$ and $\text{diag}\left(e^{-j\gamma^v}, e^{-j\gamma^h}\right)$ in (2) represent the precoder at the AP and combiner at the user, respectively. In (2), because of the single RF chain, the total transmission power P_t is divided equally between the two radiated polarizations. Subsequently, the polarization signals are combined at the receive DP antenna as

$$\begin{aligned} y &= y^v + y^h \\ &= \left(e^{-j\gamma^v} \left\{ (h_r^{vv})^* \omega^{vv} e^{-j\phi^{vv}} g^{vv} + (h_r^{hv})^* \omega^{hv} e^{-j\phi^{hv}} g^{hv} + (h_d^v)^* \right\} \frac{P_t}{2} e^{-j\theta^v} x \right) \\ &\quad + \left(e^{-j\gamma^h} \left\{ (h_r^{vh})^* \omega^{vh} e^{-j\phi^{vh}} g^{vh} + (h_r^{hh})^* \omega^{hh} e^{-j\phi^{hh}} g^{hh} + (h_d^h)^* \right\} \frac{P_t}{2} e^{-j\theta^h} x \right), \end{aligned} \quad (2a)$$

where $(h_r^{pp})^* \omega^{pp} e^{-j\phi^{pp}} g^{pp}$, $p \in \{v, h\}$, represents the total channel gain of the signal, which traverses through the polarization p of the AP-IRS link and is subsequently reflected towards the polarization p , $p \in \{v, h\}$, of the IRS-User link. This reflection occurs without any polarization conversion and is then focused on the corresponding p , $p \in \{v, h\}$, component of the receive DP antenna. In contrast, in (2), $(h_r^{pq})^* \omega^{pq} e^{-j\phi^{pq}} g^{pq}$, $p, q \in \{v, h\}$, $p \neq q$, represents the total channel gain in the reflected path involving the conversion of the signal, which traverses through the polarization p to the polarization q . This reflected signal is directed towards the polarization q of the IRS-User link.

It is noteworthy that (2a) pertains to a single-input single-output system, wherein a single transmit/receive DP antenna is accompanied by a single RF chain. In such a configuration, the deployment of DP-IRS and DP antennas only achieves the PD gains, while providing no PM gains. Nonetheless, upon extending this model to encompass MIMO scenarios, where an array of DP antennas and multiple data streams are available, the beam splitting and polarization

conversion capabilities of DP-IRS supplement the PD gains. This facilitates more effective control of the split orthogonal beams in the IRS-User links and the beams emanating from the AP-User links; consequently resulting in the interlayer multiplexing gains.

The signal model given in (2a) can be extended to N_t transmit antennas, N_r receive antennas, and N reflecting elements as

$$\begin{aligned} \mathbf{y} = \mathbf{W} & \left[\mathbf{E}_v \left\{ \mathbf{H}_{r,vv}^H \Theta_{vv} \mathbf{G}_{vv} + \mathbf{H}_{r,hv}^H \Theta_{hv} \mathbf{G}_{hv} + \mathbf{H}_{d,v}^H \right\} \mathbf{U}_v \right. \\ & \left. + \mathbf{E}_h \left\{ \mathbf{H}_{r,hh}^H \Theta_{hh} \mathbf{G}_{hh} + \mathbf{H}_{r,vh}^H \Theta_{vh} \mathbf{G}_{vh} + \mathbf{H}_{d,h}^H \right\} \mathbf{U}_h \right] \mathbf{F} \mathbf{s} + \mathbf{W} \mathbf{z}, \end{aligned} \quad (3)$$

where \mathbf{z} and \mathbf{s} represent a circularly symmetric complex Gaussian noise vector at the user and the transmitted symbol vector at the AP, respectively. In addition, $\mathbf{F} \in \mathbb{C}^{N_t \times N_s}$ and $\mathbf{W} \in \mathbb{C}^{N_r \times N_s}$ denote the precoding and combining matrices at the AP and user, respectively. The matrices $\mathbf{E}_v \in \mathbb{C}^{N_r \times N_r}$, $\mathbf{E}_h \in \mathbb{C}^{N_r \times N_r}$, $\mathbf{U}_v \in \mathbb{C}^{N_t \times N_t}$, and $\mathbf{U}_h \in \mathbb{C}^{N_t \times N_t}$ contain the receive vertical, receive horizontal, transmit vertical, transmit horizontal phase shifters in the diagonal, respectively, i.e., $\mathbf{E}_p = \text{diag}(e^{-j\gamma_{p,1}}, e^{-j\gamma_{p,2}}, e^{-j\gamma_{p,3}}, \dots, e^{-j\gamma_{p,N_r}})$ and $\mathbf{U}_p = \text{diag}(e^{-j\theta_{p,1}}, e^{-j\theta_{p,2}}, e^{-j\theta_{p,3}}, \dots, e^{-j\theta_{p,N_t}})$, where $p \in \{v, h\}$. The baseband equivalent channels of the AP-IRS, IRS-User, and AP-User links are denoted as $\mathbf{G} \in \mathbb{C}^{N \times N_t}$, $\mathbf{H}_r^H \in \mathbb{C}^{N_r \times N}$, and $\mathbf{H}_d^H \in \mathbb{C}^{N_r \times N_t}$, respectively.

Note that, in addition to the allocation of the optimal power to each DP antenna, which is further equally divided between two polarizations, \mathbf{F} is employed as a common beamformer for both the polarizations of each DP antenna. Nevertheless, when combined with the transmit phase shifters, it generates a different effective beamformer $\mathbf{U}_v \mathbf{F}$ and $\mathbf{U}_h \mathbf{F}$ for each polarization. Similarly, the operation of \mathbf{W} combined with the receive phase shifters of each polarization, $\mathbf{W} \mathbf{E}_v$ and $\mathbf{W} \mathbf{E}_h$, can be conceptualized.

Owing to the same spatial location of each subpart of a reflecting element, we can assume the same channel between identical polarizations of the AP, DP-IRS, and user [36]. For example, the signals reflected by the vv and hv subparts of a reflecting element are directed towards the vertical parts of the receiver; hence, we can assume $\mathbf{H}_{r,vv} = \mathbf{H}_{r,hv} = \mathbf{H}_{r,v}$ [36]. Similarly, we can assume $\mathbf{H}_{r,hh} = \mathbf{H}_{r,vh} = \mathbf{H}_{r,h}$ for the IRS-User link and $\mathbf{G}_{vv} = \mathbf{G}_{vh} = \mathbf{G}_v$ and $\mathbf{G}_{hh} = \mathbf{G}_{hv} = \mathbf{G}_h$ for AP-IRS link. For the proposed work, we assume that all the elements exhibit complete reflection, which can be attained by setting $\omega^{vv} = \omega^{hv} = \omega^{vh} = \omega^{hh} = 1$ [6], [7]. The signal model in (3) is simplified as

$$\begin{aligned} \mathbf{y} = \mathbf{W} & \left[\mathbf{E}_v \left\{ \mathbf{H}_{r,v}^H (\Theta_{vv} \mathbf{G}_v + \Theta_{hv} \mathbf{G}_h) + \mathbf{H}_{d,v}^H \right\} \mathbf{U}_v \right. \\ & \left. + \mathbf{E}_h \left\{ \mathbf{H}_{r,h}^H (\Theta_{hh} \mathbf{G}_h + \Theta_{vh} \mathbf{G}_v) + \mathbf{H}_{d,h}^H \right\} \mathbf{U}_h \right] \mathbf{F} \mathbf{s} + \mathbf{W} \mathbf{z}. \end{aligned} \quad (3a)$$

To streamline our analysis and avoid complex mathematical formulations, this study does not consider the optimization of the transmit DP antennas phase shifters ($\mathbf{U}_v, \mathbf{U}_h$). Instead, we focus on the optimization of the DP-IRS's beam splitting and polarization conversion capabilities. To this end, we assume $\Theta_{vv} = \Theta_{hv}$ and $\Theta_{hh} = \Theta_{vh}$, which simplifies (3a) as

$$\begin{aligned} \mathbf{y} &= \mathbf{W} \left[\mathbf{E}_v \left\{ \mathbf{H}_{r,v}^H \Theta_{hv} \mathbf{G}_v + \mathbf{H}_{r,v}^H \Theta_{hv} \mathbf{G}_h + \mathbf{H}_{d,v}^H \right\} \right. \\ &\quad \left. + \mathbf{E}_h \left\{ \mathbf{H}_{r,h}^H \Theta_{vh} \mathbf{G}_v + \mathbf{H}_{r,h}^H \Theta_{vh} \mathbf{G}_h + \mathbf{H}_{d,h}^H \right\} \right] \mathbf{F} \mathbf{s} + \mathbf{W} \mathbf{z}, \\ &= \mathbf{W} \left[\mathbf{E}_v \left\{ \mathbf{H}_{r,v}^H \Theta_{hv} \mathbf{G} + \mathbf{H}_{d,v}^H \right\} + \mathbf{E}_h \left\{ \mathbf{H}_{r,h}^H \Theta_{vh} \mathbf{G} + \mathbf{H}_{d,h}^H \right\} \right] \mathbf{F} \mathbf{s} + \mathbf{W} \mathbf{z}, \end{aligned} \quad (4)$$

where $\mathbf{G} = \mathbf{G}_v + \mathbf{G}_h$.

It is pertinent to observe that although we do not specifically optimize $(\Theta_{vv}, \Theta_{hh})$ and $(\mathbf{U}_v, \mathbf{U}_h)$ in this work, our proposed algorithms can be readily extended to accommodate them. In addition, the energy normalization factor in the signal model is neglected. However, the incorporation of a factor of $\frac{1}{\sqrt{2}}$ in (1) would resolve the normalization issue. It is also noteworthy that our simplifications result in a decline in the PD and combining gains in the system. Consequently, the gains of the DP-IRS over S-IRS presented in Section V can be regarded as the minimum gains. Further details on the gains of the DP-IRS over S-IRS are provided in Section V.

Let $\mathbf{H} = \mathbf{E}_v \left\{ \mathbf{H}_{r,v}^H \Theta_v \mathbf{G} + \mathbf{H}_{d,v}^H \right\} + \mathbf{E}_h \left\{ \mathbf{H}_{r,h}^H \Theta_h \mathbf{G} + \mathbf{H}_{d,h}^H \right\}$ denote a composite MIMO channel, where Θ_v and Θ_h represent Θ_{hv} and Θ_{vh} , respectively, for notational brevity. Then, the spectral efficiency of the system is given by

$$c = \log_2 \det \left(\mathbf{I} + \frac{1}{\sigma^2} \mathbf{W}^\dagger \mathbf{H} \mathbf{F} \mathbf{F}^H \mathbf{H}^H \mathbf{W} \right) \text{ bps/Hz}, \quad (5)$$

where \mathbf{I} denotes an identity matrix of an appropriate size and σ^2 is the noise variance. Correspondingly, the capacity maximization problem can be formulated as:

$$\begin{aligned} &\max_{\mathbf{W}, \mathbf{F}, \mathbf{E}_v, \mathbf{E}_h, \Theta_v, \Theta_h} \log_2 \det \left(\mathbf{I} + \frac{1}{\sigma^2} \mathbf{W}^\dagger \mathbf{H} \mathbf{F} \mathbf{F}^H \mathbf{H}^H \mathbf{W} \right) \\ \text{s.t.} \quad &\mathbf{H} = \mathbf{E}_v \left\{ \mathbf{H}_{r,v}^H \Theta_v \mathbf{G} + \mathbf{H}_{d,v}^H \right\} + \mathbf{E}_h \left\{ \mathbf{H}_{r,h}^H \Theta_h \mathbf{G} + \mathbf{H}_{d,h}^H \right\}, \\ &\Theta_p = \text{diag}(e^{-j\phi_{p,1}}, e^{-j\phi_{p,2}}, e^{-j\phi_{p,3}}, \dots, e^{-j\phi_{p,N}}), p \in \{v, h\}, \\ &\mathbf{E}_p = \text{diag}(e^{-j\gamma_{p,1}}, e^{-j\gamma_{p,2}}, e^{-j\gamma_{p,3}}, \dots, e^{-j\gamma_{p,N_r}}), p \in \{v, h\}, \\ &\|\mathbf{F}\|^2 = \frac{P_t}{2}. \end{aligned} \quad (P1)$$

The objective function of (P1) can be demonstrated to be a non-concave over $\mathbf{E}_v, \mathbf{E}_h, \Theta_v$, and Θ_h . Moreover, the unimodular restrictions in the second and third constraints of (P1) are nonconvex. In general, there is no standard method for solving (P1) optimally. In the following two sections, we propose three AO-based algorithms to efficiently solve this problem.

III. PROPOSED SOLUTION TO PROBLEM (P1)

Here, we describe the framework of the proposed algorithm. Specifically, we first divide the problem (P1) into several non-convex subproblems, which are solved separately. Then, we propose the AO algorithm, which solves the subproblems alternately until the objective function converges.

A. Optimal Precoder, Combiner, and Number of Data Streams

Here, we reformulate the problem (P1) to find the optimal precoder, combiner, and number of data streams for the system. For formulation, we assume $\mathbf{E}_v = \mathbf{E}_h = \mathbf{\Theta}_v = \mathbf{\Theta}_h = \mathbf{I}$. Correspondingly, the problem (P1) is written as

$$\begin{aligned} \max_{\mathbf{W}, \mathbf{F}} \quad & \log_2 \det(\mathbf{I} + \frac{1}{\sigma^2} \mathbf{W}^\dagger \mathbf{H}_I \mathbf{F} \mathbf{F}^H \mathbf{H}_I^H \mathbf{W}) \\ \text{s.t.} \quad & \mathbf{H}_I = \mathbf{H}_{r,v}^H \mathbf{G} + \mathbf{H}_{d,v}^H + \mathbf{H}_{r,h}^H \mathbf{G} + \mathbf{H}_{d,h}^H, \\ & \|\mathbf{F}\|^2 = \frac{P_t}{2}. \end{aligned} \quad (\text{P1.1})$$

Problem (P1.1) is a conventional MIMO capacity maximization problem that can be solved by singular value decomposition (SVD) and the water-filling power allocation technique [37]. Let $\text{svd}(\mathbf{H}_I) = \mathbf{U} \mathbf{\Sigma} \mathbf{V}^H$, where $\mathbf{V} \in \mathbb{C}^{N_t \times R}$ with $\text{rank}(\mathbf{H}_I) \leq \min(N_t, N_r)$ denotes the maximum number of data streams that can be transferred over \mathbf{H}_I . The optimal precoder \mathbf{F} and combiner \mathbf{W} can be written as: $\mathbf{F} = \mathbf{V} \mathbf{\Gamma}^{\frac{1}{2}}$ and $\mathbf{W} = \mathbf{U}$, respectively, where $\mathbf{\Gamma} = \text{diag}(\rho_1, \rho_2, \dots, \rho_{N_s})$ is an $N_s \times N_s$ diagonal matrix with ρ_{n_s} being the transmit power allocated to the n_s th data stream, $n_s = 1, 2, \dots, N_s$, which is determined by the water-filling power allocation such that $\sum_{n_s=1}^{N_s} \rho_{n_s} \leq \frac{P_t}{2}$. By inserting \mathbf{F} and \mathbf{W} into (P1), the problem for $\mathbf{\Theta}_v$, $\mathbf{\Theta}_h$, \mathbf{E}_v , and \mathbf{E}_h can be expressed as

$$\begin{aligned} \max_{\mathbf{\Theta}_v, \mathbf{\Theta}_h, \mathbf{E}_v, \mathbf{E}_h} \quad & \sum_{n_s=1}^{N_s} \log_2 \left(1 + \frac{1}{\sigma^2} \left| \mathbf{w}_{n_s}^* \left\{ \mathbf{E}_v (\mathbf{H}_{r,v}^H \mathbf{\Theta}_v \mathbf{G} + \mathbf{H}_{d,v}^H) + \mathbf{E}_h (\mathbf{H}_{r,h}^H \mathbf{\Theta}_h \mathbf{G} + \mathbf{H}_{d,h}^H) \right\} \mathbf{f}_{n_s} \right|^2 \right) \\ \text{s.t.} \quad & \mathbf{\Theta}_p = \text{diag}(e^{-j\phi_{p,1}}, e^{-j\phi_{p,2}}, e^{-j\phi_{p,3}}, \dots, e^{-j\phi_{p,N}}), p \in \{v, h\}, \\ & \mathbf{E}_p = \text{diag}(e^{-j\gamma_{p,1}}, e^{-j\gamma_{p,2}}, e^{-j\gamma_{p,3}}, \dots, e^{-j\gamma_{p,N_r}}), p \in \{v, h\}, \\ & \|\mathbf{f}_{n_s}\|^2 = \frac{\rho_{n_s}}{2}, n_s = 1, 2, \dots, N_s, \end{aligned} \quad (\text{P1.2})$$

where the objective function is the summation of the spectral efficiencies provided by N_s data streams [32]. The problem (P1.2) is a non-convex optimization problem with a non-concave objective function. In the next two subsections, we solve (P1.2) for $(\mathbf{\Theta}_v, \mathbf{\Theta}_h)$ and $(\mathbf{E}_v, \mathbf{E}_h)$.

B. DP-IRS Phases Optimization

By assuming $\mathbf{E}_v = \mathbf{E}_h = \mathbf{I}$, the problem (P1.2) can be written as

$$\begin{aligned} \max_{\Theta_v, \Theta_h} \quad & \sum_{n_s=1}^{N_s} \log_2 \left(1 + \frac{1}{\sigma^2} |\mathbf{w}_{n_s}^* \{ \mathbf{H}_{r,v}^H \Theta_v \mathbf{G} + \mathbf{H}_{d,v}^H + \mathbf{H}_{r,h}^H \Theta_h \mathbf{G} + \mathbf{H}_{d,h}^H \} \mathbf{f}_{n_s}|^2 \right) \\ \text{s.t.} \quad & \Theta_p = \text{diag}(e^{-j\phi_{p,1}}, e^{-j\phi_{p,2}}, e^{-j\phi_{p,3}}, \dots, e^{-j\phi_{p,N}}), p \in \{v, h\}, \\ & \|\mathbf{f}_{n_s}\|^2 = \rho_{n_s}, n_s = 1, 2, \dots, N_s. \end{aligned} \quad (\text{P1.3})$$

By the change of variables $\mathbf{w}_{n_s}^* \mathbf{H}_{d,p}^H \mathbf{f}_{n_s} = \beta_{p,n_s}$, $\mathbf{w}_{n_s}^* \mathbf{H}_{r,p}^H \Theta_p \mathbf{G} \mathbf{f}_{n_s} = \mathbf{l}_p^H \boldsymbol{\alpha}_{p,n_s}$, where $\mathbf{l}_p^H = [e^{-j\phi_{p,1}}, e^{-j\phi_{p,2}}, e^{-j\phi_{p,3}}, \dots, e^{-j\phi_{p,N}}]$, $\boldsymbol{\alpha}_{p,n_s} = \text{diag}(\mathbf{w}_{n_s}^* \mathbf{H}_{r,p}^H) \mathbf{G} \mathbf{f}_{n_s}$, and $p \in \{v, h\}$, (P1.3) is rewritten as

$$\begin{aligned} \max_{\mathbf{l}_v, \mathbf{l}_h} \quad & \sum_{n_s=1}^{N_s} \log_2 \left(1 + \frac{1}{\sigma^2} |\mathbf{l}_v^H \boldsymbol{\alpha}_{v,n_s} + \mathbf{l}_h^H \boldsymbol{\alpha}_{h,n_s} + \beta_{v,n_s} + \beta_{h,n_s}|^2 \right) \\ \text{s.t.} \quad & |\mathbf{l}_{n,p}| = 1, \quad n = 1, \dots, N, \quad p \in \{v, h\}. \end{aligned} \quad (\text{P1.4})$$

Next, we solve the problems (P1.4) for \mathbf{l}_v and \mathbf{l}_h , separately.

1) *Optimization of Vertical Phase Shifts:* Here, we solve (P1.4) for \mathbf{l}_v . Let $\mathbf{l}_h = [1, 1, \dots, 1]$ and $\mathbf{l}_h^H \boldsymbol{\alpha}_{h,n_s} + \beta_{v,n_s} + \beta_{h,n_s} = \eta_{v,n_s}$. (P1.4) can be written as

$$\begin{aligned} \max_{\mathbf{l}_v} \quad & \sum_{n_s=1}^{N_s} \log_2 \left(1 + \frac{1}{\sigma^2} |\mathbf{l}_v^H \boldsymbol{\alpha}_{v,n_s} + \eta_{v,n_s}|^2 \right) \\ \text{s.t.} \quad & |\mathbf{l}_{n,v}| = 1, \quad n = 1, \dots, N. \end{aligned} \quad (\text{P1.5})$$

Despite being simplified, problem (P1.5) remains a nonconvex optimization problem with a nonconcave objective function and nonconvex unit modulus constraint. Nevertheless, we convert (P1.5) into a semi-definite program using the SDR method, which can be efficiently performed by a CVX solver [38]. Inserting $|\mathbf{l}_v^H \boldsymbol{\alpha}_{v,n_s} + \eta_{v,n_s}|^2 = \mathbf{l}_v^H \boldsymbol{\alpha}_{v,n_s} \boldsymbol{\alpha}_{v,n_s}^H \mathbf{l}_v + \mathbf{l}_v^H \boldsymbol{\alpha}_{v,n_s} \eta_{v,n_s}^H + \eta_{v,n_s} \boldsymbol{\alpha}_{v,n_s}^H \mathbf{l}_v + |\eta_{v,n_s}|^2$ in (P1.5), we have

$$\begin{aligned} \max_{\mathbf{l}_v} \quad & \sum_{n_s=1}^{N_s} \log_2 \left(1 + \frac{1}{\sigma^2} \{ \mathbf{l}_v^H \boldsymbol{\alpha}_{v,n_s} \boldsymbol{\alpha}_{v,n_s}^H \mathbf{l}_v + \mathbf{l}_v^H \boldsymbol{\alpha}_{v,n_s} \eta_{v,n_s}^H + \eta_{v,n_s} \boldsymbol{\alpha}_{v,n_s}^H \mathbf{l}_v + |\eta_{v,n_s}|^2 \} \right) \\ \text{s.t.} \quad & |\mathbf{l}_{n,v}| = 1, \quad n = 1, \dots, N. \end{aligned} \quad (\text{P1.6})$$

By defining $\mathbf{O}_{v,n_s} = \begin{bmatrix} \boldsymbol{\alpha}_{v,n_s} \boldsymbol{\alpha}_{v,n_s}^H & \boldsymbol{\alpha}_{v,n_s} \eta_{v,n_s}^H \\ \boldsymbol{\alpha}_{v,n_s}^H \eta_{v,n_s} & 0 \end{bmatrix}$ and $\bar{\mathbf{l}}_v = \begin{bmatrix} \mathbf{l}_v \\ \psi \end{bmatrix}$, where ψ is an auxiliary variable, (P1.6) can be homogenized [7] as

$$\begin{aligned} \max_{\bar{\mathbf{l}}_v} \quad & \sum_{n_s=1}^{N_s} \log_2 \left(1 + \frac{1}{\sigma^2} \{ \bar{\mathbf{l}}_v^H \mathbf{O}_{v,n_s} \bar{\mathbf{l}}_v + |\eta_{v,n_s}|^2 \} \right) \\ \text{s.t.} \quad & |\bar{\mathbf{l}}_{n,v}| = 1, \quad n = 1, \dots, N+1. \end{aligned} \quad (\text{P1.7})$$

In (P1.7), we insert $\bar{\mathbf{I}}_h^{-H} \mathbf{O}_{v,n_s} \bar{\mathbf{I}}_v = \text{trace}(\mathbf{O}_{v,n_s} \mathbf{L}_v)$, where $\mathbf{L}_v = \bar{\mathbf{I}}_v \bar{\mathbf{I}}_h^{-H}$ must satisfy the constraints $\mathbf{L}_v \succeq 0$ and $\text{rank}(\mathbf{L}_v) = 1$, we have

$$\begin{aligned} & \max_{\mathbf{L}_v} \sum_{n_s=1}^{N_s} \log_2 \left(1 + \frac{1}{\sigma^2} (\text{trace}(\mathbf{O}_{v,n_s} \mathbf{L}_v) + |\eta_{v,n_s}|^2) \right) \\ \text{s.t.} \quad & \mathbf{L}_{(n,n),v} = 1, \quad n = 1, \dots, N+1, \\ & \mathbf{L}_v \succeq 0, \\ & \text{rank}(\mathbf{L}_v) = 1. \end{aligned} \tag{P1.8}$$

Although the objective function is concave, the problem (P1.8) remains a non-convex optimization problem because of the non-convex rank-one constraint, i.e., $\text{rank}(\mathbf{L}_v) = 1$. Relaxing this constraint, (P1.8) is given by

$$\begin{aligned} & \max_{\mathbf{L}_v} \sum_{n_s=1}^{N_s} \log_2 \left(1 + \frac{1}{\sigma^2} (\text{trace}(\mathbf{O}_{v,n_s} \mathbf{L}_v) + |\eta_{v,n_s}|^2) \right) \\ \text{s.t.} \quad & \mathbf{L}_{(n,n),v} = 1, \quad n = 1, \dots, N+1, \\ & \mathbf{L}_v \succeq 0. \end{aligned} \tag{P1.9}$$

The problem (P1.9) is a convex optimization problem that can be solved using a CVX solver [38]; however, two issues remain with its formulation.

- 1) Solving (P1.9) does not guarantee that the objective value, i.e., $\sum_{n_s=1}^{N_s} \log_2 \left(1 + \frac{1}{\sigma^2} (\text{trace}(\mathbf{O}_{v,n_s} \mathbf{L}_v) + |\eta_{v,n_s}|^2) \right)$, monotonically increases in each iteration of the AO algorithm, which may result in the non-convergence behaviors of the algorithm.
- 2) Because of the objective function and last constraint, i.e., log-sum expression in (P1.9), which belongs to the functions of the exponential family, using a CVX solver to solve (P1.9) is excessively slow. More details on this issue are presented in [39].

To address the first issue, we introduce another constraint and update (P1.9) as follows:

$$\begin{aligned} & \max_{\mathbf{L}_v} \sum_{n_s=1}^{N_s} \log_2 \left(1 + \frac{1}{\sigma^2} (\text{trace}(\mathbf{O}_{v,n_s} \mathbf{L}_v) + |\eta_{v,n_s}|^2) \right) \\ \text{s.t.} \quad & \mathbf{L}_{v(n,n)} = 1, \quad n = 1, \dots, N+1, \\ & \mathbf{L}_v \succeq 0, \\ & \sum_{n_s=1}^{N_s} \log_2 \left(1 + \frac{1}{\sigma^2} (\text{trace}(\mathbf{O}_{v,n_s} \mathbf{L}_v) + |\eta_{v,n_s}|^2) \right) \geq \lambda_{\mathbf{L}_v}, \end{aligned} \tag{P1.10}$$

where $\lambda_{\mathbf{L}_v}$ represents a positive real number chosen in each iteration of AO, such that the objective value remains non-decreasing and guarantees convergence. More details on the selection of $\lambda_{\mathbf{L}_v}$ are provided in Section IV-D.

To address the second issue, the log-sum expressions in (P1.10) must be discarded. In [39], it is demonstrated that an optimization problem involving the log-sum expression can be replaced with the geometric mean. Specifically, let

$\mathbf{x}_{\mathbf{L}_v} = \left[\left(1 + \frac{1}{\sigma^2} (\text{trace}(\mathbf{O}_{v,1}\mathbf{L}_v) + |\eta_{v,1}|^2) \right), \dots, \left(1 + \frac{1}{\sigma^2} (\text{trace}(\mathbf{O}_{v,n_s}\mathbf{L}_v) + |\eta_{v,n_s}|^2) \right) \right]$ be a vector containing the $1 + \text{SNR}$ value of each data stream, then the objective function $\text{logsum}(\mathbf{x})$ and constraint $\text{logsum}(\mathbf{x}) \geq \lambda_{\mathbf{L}_v}$ in (P1.10) can be replaced by $\text{GM}(\mathbf{x})$ and $\text{GM}(\mathbf{x}) \geq (\log(\lambda_{\mathbf{L}_v}))^{\frac{1}{\text{length}(\mathbf{x})}} = (\log(\lambda_{\mathbf{L}_v}))^{\frac{1}{N_s}} = \lambda'_{\mathbf{L}_v}$, respectively. Consequently, we have

$$\begin{aligned} \max_{\mathbf{L}_v} \quad & \text{GM}(\mathbf{x}_{\mathbf{L}_v}) \\ \text{s.t.} \quad & \mathbf{x}_{\mathbf{L}_v} = \left[\left(1 + \frac{1}{\sigma^2} (\text{trace}(\mathbf{O}_{v,1}\mathbf{L}_v) + |\eta_{v,1}|^2) \right), \dots, \left(1 + \frac{1}{\sigma^2} (\text{trace}(\mathbf{O}_{v,n_s}\mathbf{L}_v) + |\eta_{v,n_s}|^2) \right) \right] \\ & \mathbf{L}_{v(n,n)} = 1, \quad n = 1, \dots, N + 1, \\ & \mathbf{L}_v \succeq 0, \\ & \text{GM}(\mathbf{x}_{\mathbf{L}_v}) \geq \lambda'_{\mathbf{L}_v}. \end{aligned} \tag{P1.11}$$

Note that (P1.11) can be written in a simpler form, which is a feasibility check problem without any objective function, as

$$\begin{aligned} \text{find} \quad & \mathbf{L}_v \\ \text{s.t.} \quad & \mathbf{x}_{\mathbf{L}_v} = \left[\left(1 + \frac{1}{\sigma^2} (\text{trace}(\mathbf{O}_{v,1}\mathbf{L}_v) + |\eta_{v,1}|^2) \right), \dots, \left(1 + \frac{1}{\sigma^2} (\text{trace}(\mathbf{O}_{v,n_s}\mathbf{L}_v) + |\eta_{v,n_s}|^2) \right) \right] \\ & \mathbf{L}_{v(n,n)} = 1, \quad n = 1, \dots, N + 1, \\ & \mathbf{L}_v \succeq 0, \\ & \text{GM}(\mathbf{x}_{\mathbf{L}_v}) \geq \lambda'_{\mathbf{L}_v}. \end{aligned} \tag{P1.12}$$

However, because there is no objective function, solving (P1.12) requires more iterations than solving (P1.11) for the convergence of the AO algorithm, as will be demonstrated in Section VI. To accumulate the benefits of (P1.11) and (P1.12), i.e., simpler formulation and fewer iterations, into one formulation, we introduce a slack variable $\xi_{\mathbf{L}_v}$ and reformulate the problem (P1.12) as

$$\begin{aligned} \max_{\mathbf{L}_v} \quad & \xi_{\mathbf{L}_v} \\ \text{s.t.} \quad & \mathbf{x}_{\mathbf{L}_v} = \left[\left(1 + \frac{1}{\sigma^2} (\text{trace}(\mathbf{O}_{v,1}\mathbf{L}_v) + |\eta_{v,1}|^2) \right), \dots, \left(1 + \frac{1}{\sigma^2} (\text{trace}(\mathbf{O}_{v,n_s}\mathbf{L}_v) + |\eta_{v,n_s}|^2) \right) \right] \\ & \mathbf{L}_{v(n,n)} = 1, \quad n = 1, \dots, N + 1, \\ & \mathbf{L}_v \succeq 0, \\ & \text{GM}(\mathbf{x}_{\mathbf{L}_v}) \geq \lambda'_{\mathbf{L}_v} + \xi_{\mathbf{L}_v}. \end{aligned} \tag{P1.13}$$

The formulation of (P1.13) is simpler than that of (P1.11), and solving it requires fewer iterations than (P1.12). More details regarding the convergence behaviors and time complexities of these formulations are provided in Section VI. Solving (P1.13) may result in a higher-rank solution; hence, retrieving Θ_v from \mathbf{L}_v might require more steps, i.e., Gaussian randomization. Details are provided in [40].

2) *Optimization of Horizontal Phase Shifts:* Let $\mathbf{l}_v^H \boldsymbol{\alpha}_{v,n_s} + \beta_{v,n_s} + \beta_{h,n_s} = \eta_{h,n_s}$, where \mathbf{l}_v is retrieved from \mathbf{L}_v by solving (P1.11). Then the problem (P1.4) for \mathbf{l}_h can be written as

$$\begin{aligned} \max_{\mathbf{l}_h} \quad & \sum_{n_s=1}^{N_s} \log_2 \left(1 + \frac{1}{\sigma^2} |\mathbf{l}_h^H \boldsymbol{\alpha}_{v,n_s} + \eta_{h,n_s}|^2 \right) \\ \text{s.t.} \quad & |\mathbf{l}_{n,h}| = 1, \quad n = 1, \dots, N. \end{aligned} \quad (\text{P1.14})$$

Following the steps similar to those for the vertical polarization phases, we obtain an equivalent formulation for (P1.14) as

$$\begin{aligned} \max_{\mathbf{L}_h} \quad & \xi_{\mathbf{L}_h} \\ \text{s.t.} \quad & \mathbf{x}_{\mathbf{L}_h} = \left[\left(1 + \frac{1}{\sigma^2} (\text{trace}(\mathbf{O}_{h,1} \mathbf{L}_h) + |\eta_{h,1}|^2) \right), \dots, \left(1 + \frac{1}{\sigma^2} (\text{trace}(\mathbf{O}_{h,N_s} \mathbf{L}_h) + |\eta_{h,N_s}|^2) \right) \right] \\ & \mathbf{L}_{h(n,n)} = 1, \quad n = 1, \dots, N+1, \\ & \mathbf{L}_h \succeq 0, \\ & \text{GM}(\mathbf{x}_{\mathbf{L}_h}) \geq \lambda'_{\mathbf{L}_h} + \xi_{\mathbf{L}_h}, \end{aligned} \quad (\text{P1.15})$$

where $\mathbf{O}_{h,n_s} = \begin{bmatrix} \boldsymbol{\alpha}_{h,n_s} \boldsymbol{\alpha}_{h,n_s}^H & \boldsymbol{\alpha}_{h,n_s} \eta_{h,n_s}^H \\ \boldsymbol{\alpha}_{h,n_s}^H \eta_{h,n_s} & 0 \end{bmatrix}$, $\mathbf{L}_h = \overline{\mathbf{l}}_h \overline{\mathbf{l}}_h^H$, $\overline{\mathbf{l}}_h = \begin{bmatrix} \mathbf{l}_h \\ \psi \end{bmatrix}$, ψ is a auxiliary variable, $\xi_{\mathbf{L}_h}$ is a slack variable, and $\lambda'_{\mathbf{L}_h}$ is positive real number.

C. Optimal Phase Shifters for Receive DP Antennas

Given Θ_v and Θ_h from (P1.13) and (P1.15), respectively, the problem (P1.2) for \mathbf{E}_v and \mathbf{E}_h can be rewritten as

$$\begin{aligned} \max_{\mathbf{E}_v, \mathbf{E}_h} \quad & \sum_{n_s=1}^{N_s} \log_2 \left(1 + \frac{1}{\sigma^2} |\mathbf{w}_{n_s}^* \mathbf{E}_v \mathbf{h}_{v,n_s} + \mathbf{w}_{n_s}^* \mathbf{E}_h \mathbf{h}_{h,n_s}|^2 \right) \\ \text{s.t.} \quad & \mathbf{E}_p = \text{diag}(e^{-j\gamma_{p,1}}, e^{-j\gamma_{p,2}}, e^{-j\gamma_{p,3}}, \dots, e^{-j\gamma_{p,N_r}}), \quad p \in \{v, h\} \\ & \mathbf{h}_{p,n_s} = \mathbf{H}_{r,p}^H \Theta_p \mathbf{G} \mathbf{f}_{n_s} + \mathbf{H}_{d,p}^H \mathbf{f}_{n_s}, \quad p \in \{v, h\} \\ & \|\mathbf{f}_{n_s}\|^2 = \rho_{n_s}, \quad n_s = 1, 2, \dots, N_s. \end{aligned} \quad (\text{P1.16})$$

By applying the change of variables $\mathbf{w}_{n_s}^* \mathbf{E}_p \mathbf{h}_{p,n_s} = \mathbf{e}_p^T \mathbf{h}'_{p,n_s}$, where $\mathbf{h}'_{p,n_s} = \text{diag}(\mathbf{w}_{n_s}^*) \cdot \mathbf{h}_{p,n_s}$, $\mathbf{e}_p^T = [e^{-j\gamma_{p,1}}, e^{-j\gamma_{p,2}}, e^{-j\gamma_{p,3}}, \dots, e^{-j\gamma_{p,N_r}}]$, and $p \in \{v, h\}$, (P1.16) is reduced to

$$\begin{aligned} \max_{\mathbf{e}_v, \mathbf{e}_h} \quad & \sum_{n_s=1}^{N_s} \log_2 \left(1 + \frac{1}{\sigma^2} |\mathbf{e}_v^T \mathbf{h}'_{v,n_s} + \mathbf{e}_h^T \mathbf{h}'_{h,n_s}|^2 \right) \\ \text{s.t.} \quad & \mathbf{e}_p^T = [e^{-j\gamma_{p,1}}, e^{-j\gamma_{p,2}}, e^{-j\gamma_{p,3}}, \dots, e^{-j\gamma_{p,N_r}}], \quad p \in \{v, h\} \\ & \mathbf{h}'_{p,n_s} = \text{diag}(\mathbf{w}_{n_s}^*) \cdot \mathbf{h}_{p,n_s}, \quad n_s = 1, 2, \dots, N_s. \end{aligned} \quad (\text{P1.17})$$

Next, we solve (P1.17) separately for \mathbf{e}_v and \mathbf{e}_h .

1) *Receive Vertical Phase Shifts Optimization:* Here, we solve the problem (P1.17) for the vertical phase shifters of the receive DP antennas. Let $\mathbf{e}_h^T = [1, 1, \dots, 1]$ and $\mathbf{e}_h^T \mathbf{h}'_{h,n_s} = \delta_{h,n_s}$, the problem (P1.17) for \mathbf{e}_v can be written as

$$\begin{aligned} \max_{\mathbf{e}_v} \quad & \sum_{n_s=1}^{N_s} \log_2 \left(1 + \frac{1}{\sigma^2} |\mathbf{e}_v^T \mathbf{h}'_{v,n_s} + \delta_{h,n_s}|^2 \right) \\ \text{s.t.} \quad & \mathbf{e}_v^T = [e^{-j\gamma_{v,1}}, e^{-j\gamma_{v,2}}, e^{-j\gamma_{v,3}}, \dots, e^{-j\gamma_{v,N_r}}], \\ & \mathbf{h}'_{v,n_s} = \text{diag}(\mathbf{w}_{n_s}^*) \cdot \mathbf{h}_{v,n_s}, \quad n_s = 1, 2, \dots, N_s. \end{aligned} \quad (\text{P1.18})$$

Inserting $|\mathbf{e}_v^T \mathbf{h}'_{v,n_s} + \delta_{h,n_s}|^2 = \mathbf{e}_v^T \mathbf{h}'_{v,n_s} \mathbf{h}'_{v,n_s}{}^H \mathbf{e}_v^* + \mathbf{e}_v^T \mathbf{h}'_{v,n_s} \delta_{h,n_s}^H + \delta_{h,n_s} \mathbf{h}'_{v,n_s}{}^H \mathbf{e}_v^* + |\delta_{h,n_s}|^2$ in (P1.18), we have

$$\begin{aligned} \max_{\mathbf{e}_v} \quad & \sum_{n_s=1}^{N_s} \log_2 \left(1 + \frac{1}{\sigma^2} (\mathbf{e}_v^T \mathbf{h}'_{v,n_s} \mathbf{h}'_{v,n_s}{}^H \mathbf{e}_v^* + \mathbf{e}_v^T \mathbf{h}'_{v,n_s} \delta_{h,n_s}^H + \delta_{h,n_s} \mathbf{h}'_{v,n_s}{}^H \mathbf{e}_v^* + |\delta_{h,n_s}|^2) \right) \\ \text{s.t.} \quad & \mathbf{e}_v^T = [e^{-j\gamma_{v,1}}, e^{-j\gamma_{v,2}}, e^{-j\gamma_{v,3}}, \dots, e^{-j\gamma_{v,N_r}}], \\ & \mathbf{h}'_{v,n_s} = \text{diag}(\mathbf{w}_{n_s}^*) \cdot \mathbf{h}_{v,n_s}, \quad n_s = 1, 2, \dots, N_s. \end{aligned} \quad (\text{P1.19})$$

Similar to (P1.5), by defining $\mathbf{S}_{n_s}^v = \begin{bmatrix} \mathbf{h}'_{v,n_s} \mathbf{h}'_{v,n_s}{}^H & \mathbf{h}'_{v,n_s} \delta_{h,n_s}^H \\ \mathbf{h}'_{v,n_s}{}^H \delta_{h,n_s} & 0 \end{bmatrix}$, $\bar{\mathbf{e}}_v^T = [\mathbf{e}_v^T \quad \psi]$, $\bar{\mathbf{\Xi}}_v = \bar{\mathbf{e}}_v^* \bar{\mathbf{e}}_v^T$, and $\bar{\mathbf{e}}_v^T \mathbf{S}_{n_s}^v \bar{\mathbf{e}}_v^* = \text{trace}(\mathbf{S}_{n_s}^v \bar{\mathbf{\Xi}}_v)$, the SDR formulation of (P1.19) can be written as

$$\begin{aligned} \max_{\bar{\mathbf{\Xi}}_v} \quad & \sum_{n_s=1}^{N_s} \log_2 \left(1 + \frac{1}{\sigma^2} (\text{trace}(\mathbf{S}_{n_s}^v \bar{\mathbf{\Xi}}_v) + |\delta_{h,n_s}|^2) \right) \\ \text{s.t.} \quad & \bar{\mathbf{\Xi}}_{v(n_r, n_r)} = 1, \quad n = 1, \dots, N_r + 1, \\ & \bar{\mathbf{\Xi}}_v \succeq 0. \end{aligned} \quad (\text{P1.20})$$

Problem (P1.20) is a convex optimization problem that can be solved by CVX [38]; however, similar to (P1.9), solving (P1.20) in each iteration of the AO algorithm does not guarantee a

non-decreasing objective value. Hence, an equivalent formulation of (P1.20) is given by

$$\begin{aligned}
& \max_{\Xi_v} \quad \xi_{\Xi_v} \\
& \text{s.t.} \quad \mathbf{x}_{\Xi_v} = \left[\left(1 + \frac{1}{\sigma^2} (\text{trace}(\mathbf{S}_1^v \Xi_v) + |\delta_{h,n_s}|^2) \right), \dots, \left(1 + \frac{1}{\sigma^2} (\text{trace}(\mathbf{S}_{n_s}^v \Xi_v) + |\delta_{h,n_s}|^2) \right) \right] \\
& \quad \Xi_{v(n_r, n_r)} = 1, \quad n = 1, \dots, N_r + 1, \\
& \quad \Xi_v \succeq 0 \\
& \quad \text{GM}(\mathbf{x}_{\Xi_v}) \geq \lambda'_{\Xi_v} + \xi_{\Xi_v},
\end{aligned} \tag{P1.21}$$

where ξ_{Ξ_v} and λ'_{Ξ_v} are a slack variable and real positive number, respectively.

2) *Receive Horizontal Phase Shifts Optimization:* By letting $\mathbf{e}_v^T \mathbf{h}'_{v,n_s} = \delta_{v,n_s}$, where \mathbf{e}_v is retrieved from Ξ_v by solving (P1.21), the problem (P1.17) for \mathbf{e}_h can be expressed as

$$\begin{aligned}
& \max_{\mathbf{e}_h} \quad \sum_{n_s=1}^{N_s} \log_2 \left(1 + \frac{1}{\sigma^2} |\mathbf{e}_h^T \mathbf{h}'_{h,n_s} + \delta_{v,n_s}|^2 \right) \\
& \text{s.t.} \quad \mathbf{e}_h^T = [e^{-j\gamma_{h,1}}, e^{-j\gamma_{h,2}}, e^{-j\gamma_{h,3}}, \dots, e^{-j\gamma_{v,N_r}}], \\
& \quad \mathbf{h}'_{h,n_s} = \text{diag}(\mathbf{w}_{n_s}^*) \cdot \mathbf{h}_{h,n_s}, \quad n_s = 1, 2, \dots, N_s.
\end{aligned} \tag{P1.22}$$

Problem (P1.22) is similar to (P1.18); hence, by following similar steps, an equivalent formulation of (P1.22) can be obtained as

$$\begin{aligned}
& \max_{\Xi_h} \quad \xi_{\Xi_h} \\
& \text{s.t.} \quad \mathbf{x}_{\Xi_h} = \left[\left(1 + \frac{1}{\sigma^2} (\text{trace}(\mathbf{S}_1^h \Xi_h) + |\delta_{v,n_s}|^2) \right), \dots, \left(1 + \frac{1}{\sigma^2} (\text{trace}(\mathbf{S}_{n_s}^h \Xi_h) + |\delta_{v,n_s}|^2) \right) \right] \\
& \quad \Xi_{h(n_r, n_r)} = 1, \quad n = 1, \dots, N_r + 1, \\
& \quad \Xi_h \succeq 0 \\
& \quad \text{GM}(\mathbf{x}) \geq \lambda'_{\Xi_h} + \xi_{\Xi_h},
\end{aligned} \tag{P1.23}$$

$$\text{where } \mathbf{S}_{n_s}^h = \begin{bmatrix} \mathbf{h}'_{h,n_s} \mathbf{h}'_{h,n_s}{}^H & \mathbf{h}'_{h,n_s} \delta_{v,n_s}^H \\ \mathbf{h}'_{h,n_s}{}^H \delta_{v,n_s} & 0 \end{bmatrix}, \quad \Xi_h = \overline{\mathbf{e}_h}^* \overline{\mathbf{e}_h}^T, \quad \text{and } \overline{\mathbf{e}_h}^T = \begin{bmatrix} \mathbf{e}_h^T & \psi \end{bmatrix}.$$

D. Overall Algorithm

The proposed AO algorithm solves (P1.1), (P1.13), (P1.15), (P1.21), and (P1.23) alternately until the objective function of (P1) converges. To maintain the monotonically non-decreasing behavior, the maximized objective value ξ in each problem is adopted as the λ' of the next problem. The overall algorithm is summarized in Algorithm 1.

Algorithm 1 SDR-based Alternating Optimization Algorithm

- 1: Set iteration $k = 0$ and initialize $\Theta_v^k = \mathbf{I}_{\Theta_v}$, $\Theta_h^k = \mathbf{I}_{\Theta_h}$, $\mathbf{E}_v^k = \mathbf{I}_{\mathbf{E}_v}$, $\mathbf{E}_h^k = \mathbf{I}_{\mathbf{E}_h}$, and $\xi_{\Xi_h}^k = 0$.
 - 2: Solve (P1.1) using the SVD and water-filling technique, and denote the optimized \mathbf{W} , \mathbf{F} , and N_s as \mathbf{W}^k , \mathbf{F}^k , and N_s^k , respectively.
 - 3: **repeat**
 - 4: Given \mathbf{E}_v^k , \mathbf{E}_h^k , and Θ_h^k , put $\lambda'_{\mathbf{L}_v} = \xi_{\Xi_h}^k$, solve (P1.13), retrieve optimal Θ_v^{k+1} from \mathbf{L}_v using Gaussian randomization, and denote the maximized objective value as $\xi_{\mathbf{L}_v}^k$.
 - 5: Given Θ_v^{k+1} , put $\lambda'_{\mathbf{L}_h} = \xi_{\mathbf{L}_v}^k$, solve (P1.15), retrieve optimal Θ_h^{k+1} from \mathbf{L}_h using Gaussian randomization, and denote the maximized objective value as $\xi_{\mathbf{L}_h}^k$.
 - 6: Given Θ_v^{k+1} , Θ_h^{k+1} , and \mathbf{E}_h^k , put $\lambda'_{\Xi_v} = \xi_{\mathbf{L}_h}^k$, solve (P1.21), retrieve optimal \mathbf{E}_v^{k+1} from Ξ_v using Gaussian randomization, and denote the maximized objective value as $\xi_{\Xi_v}^k$.
 - 7: Given \mathbf{E}_v^{k+1} , put $\lambda'_{\Xi_h} = \xi_{\Xi_v}^k$, solve (P1.23), retrieve optimal \mathbf{E}_h^{k+1} from Ξ_h using Gaussian randomization, and denote the maximized objective value as $\xi_{\Xi_h}^{k+1}$.
 - 8: Given Θ_v^{k+1} , Θ_h^{k+1} , \mathbf{E}_h^{k+1} , and \mathbf{E}_v^{k+1} , solve (P1.1) using the SVD and water-filling technique, and denote the optimized \mathbf{W} , \mathbf{F} , and N_s as \mathbf{W}^{k+1} , \mathbf{F}^{k+1} , and N_s^{k+1} , respectively.
 - 9: Update $k = k + 1$.
 - 10: **until** the objective value of (P1) converges or the maximum number of iterations are completed.
-

IV. PROPOSED SOLUTION TO PROBLEM (P1) FOR SPECIAL CASES

Here, we consider two special scenarios and propose low-complexity solutions to (P1).

A. Low-SNR regime and/or LoS scenario

In the low-SNR regime and/or LoS scenario, the optimal way to maximize the SE of a MIMO channel is to allocate all the transmit power to the strongest eigenchannel [37]. Accordingly, problem (P1.1) for the low-SNR regime can be simplified as

$$\begin{aligned}
 & \max_{\Theta_v, \Theta_h, \mathbf{E}_v, \mathbf{E}_h} \log_2 \left(1 + \frac{1}{\sigma^2} \left| \mathbf{w}_{n_s}'^* \left\{ \mathbf{E}_h (\mathbf{H}_{r,v}^H \Theta_v \mathbf{G} + \mathbf{H}_{d,v}^H) + \mathbf{E}_h (\mathbf{H}_{r,h}^H \Theta_h \mathbf{G} + \mathbf{H}_{d,h}^H) \right\} \mathbf{f}_{n_s}' \right|^2 \right) \\
 \text{s.t. } & \Theta_p = \text{diag}(e^{-j\phi_{p,1}}, e^{-j\phi_{p,2}}, e^{-j\phi_{p,3}}, \dots, e^{-j\phi_{p,N}}), p \in \{v, h\} \\
 & \mathbf{E}_p = \text{diag}(e^{-j\gamma_{p,1}}, e^{-j\gamma_{p,2}}, e^{-j\gamma_{p,3}}, \dots, e^{-j\gamma_{p,N_r}}), p \in \{v, h\} \\
 & \left\| \mathbf{f}_{n_s}' \right\|^2 = P_t,
 \end{aligned} \tag{P1.24}$$

where n'_s denotes the index of the strongest eigenchannel. Note that in (P1.24), the maximization of the SE is equivalent to the maximization of the signal strength of the n'_s th data stream. Hence, problem (P1.24) can be rewritten as

$$\begin{aligned} & \max_{\Theta_v, \Theta_h, \mathbf{E}_v, \mathbf{E}_h} \left| \mathbf{w}_{n'_s}^* \left\{ \mathbf{E}_h (\mathbf{H}_{r,v}^H \Theta_v \mathbf{G} + \mathbf{H}_{d,v}^H) + \mathbf{E}_h (\mathbf{H}_{r,h}^H \Theta_h \mathbf{G} + \mathbf{H}_{d,h}^H) \right\} \mathbf{f}_{n'_s} \right|^2 \\ \text{s.t.} \quad & \Theta_p = \text{diag}(e^{-j\phi_{p,1}}, e^{-j\phi_{p,2}}, e^{-j\phi_{p,3}}, \dots, e^{-j\phi_{p,N}}), p \in \{v, h\}, \\ & \mathbf{E}_p = \text{diag}(e^{-j\gamma_{p,1}}, e^{-j\gamma_{p,2}}, e^{-j\gamma_{p,3}}, \dots, e^{-j\gamma_{p,N_r}}), p \in \{v, h\}, \\ & \left\| \mathbf{f}_{n'_s} \right\|^2 = \frac{P_t}{2}. \end{aligned} \quad (\text{P1.25})$$

1) *DP-IRS Phases Optimization for the Low-SNR Regime:* According to (P1.25), problem (P1.5) for the low-SNR regime is given by

$$\begin{aligned} & \max_{\mathbf{l}_v} \left| \mathbf{l}_v^H \boldsymbol{\alpha}_{v,n'_s} + \eta_{v,n'_s} \right|^2 \\ \text{s.t.} \quad & \left| \mathbf{l}_{v(n)} \right| = 1, \quad n = 1, \dots, N. \end{aligned} \quad (\text{P1.26})$$

It can be demonstrated that to solve the problem (P1.26), we should have $\arg \left(\mathbf{l}_v^H \boldsymbol{\alpha}_{v,n'_s} \right) = \arg \left(\eta_{v,n'_s} \right)$. Let $\arg \left(\eta_{v,n'_s} \right) = c_v$. (P1.26) can be reformulated as

$$\begin{aligned} & \max_{\mathbf{l}_v} \left| \mathbf{l}_v^H \boldsymbol{\alpha}_{v,n'_s} \right|^2 \\ \text{s.t.} \quad & \left| \mathbf{l}_{v(n)} \right| = 1, \quad n = 1, \dots, N, \\ & \arg \left(\mathbf{l}_v^H \boldsymbol{\alpha}_{v,n'_s} \right) = c_v. \end{aligned} \quad (\text{P1.27})$$

Its not difficult to show that the optimal solution to (P1.27) is $\mathbf{l}_v^H = e^{j(c_v - \arg(\boldsymbol{\alpha}_{v,n'_s}))}$ and correspondingly, the n th phase shift for the vertical part of the DP-IRS is given by

$$\phi_{v(n)}^* = c_v - \arg \left(\boldsymbol{\alpha}_{v,n'_s(n)} \right), \quad n = 1, 2, \dots, N. \quad (6)$$

Following steps similar to those for \mathbf{l}_v in (P1.26), the problem (P1.14) for \mathbf{l}_h is expressed as

$$\begin{aligned} & \max_{\mathbf{l}_h} \left| \mathbf{l}_h^H \boldsymbol{\alpha}_{h,n'_s} \right|^2 \\ \text{s.t.} \quad & \left| \mathbf{l}_{h(n)} \right| = 1, \quad n = 1, \dots, N, \\ & \arg \left(\mathbf{l}_h^H \boldsymbol{\alpha}_{h,n'_s} \right) = c_h, \end{aligned} \quad (\text{P1.28})$$

with the optimal solution $\mathbf{l}_h^H = e^{j(c_h - \arg(\boldsymbol{\alpha}_{h,n'_s}))}$, resulting in the following n th optimal phase shift for the horizontal part of DP-IRS:

$$\phi_{h(n)}^* = c_h - \arg \left(\boldsymbol{\alpha}_{h,n'_s(n)} \right), \quad n = 1, 2, \dots, N. \quad (7)$$

2) *Optimal Phase Shifters for Receive DP Antennas:* Corresponding to (P1.25), problem (P1.18) for \mathbf{e}_v can be simplified as

$$\begin{aligned} \max_{\mathbf{e}_v} & \quad \left| \mathbf{e}_v^T \mathbf{h}'_{v,n'_s} + \delta_{h,n'_s} \right|^2 \\ \text{s.t.} & \quad \mathbf{e}_v^T = [e^{-j\gamma_{v,1}}, e^{-j\gamma_{v,2}}, e^{-j\gamma_{v,3}}, \dots, e^{-j\gamma_{v,N_r}}] \\ & \quad \mathbf{h}'_{v,n'_s} = \text{diag}(\mathbf{w}'_{n'_s}) \cdot \mathbf{h}_{v,n'_s}. \end{aligned} \quad (\text{P1.29})$$

To maximize the objective value of (P1.29) we should have $\arg(\mathbf{e}_v^T \mathbf{h}'_{v,n'_s}) = \arg(\delta_{v,n'_s})$. Let $\arg(\delta_{h,n'_s}) = u_h$, the problem (P1.29) is reformulated as

$$\begin{aligned} \max_{\mathbf{e}_v} & \quad \left| \mathbf{e}_v^T \mathbf{h}'_{v,n'_s} \right|^2 \\ \text{s.t.} & \quad \left| \mathbf{e}_{v(n_r)} \right| = 1, \quad n_r = 1, \dots, N_r, \\ & \quad \arg(\mathbf{e}_v^T \mathbf{h}'_{v,n'_s}) = u_h, \end{aligned} \quad (\text{P1.30})$$

with the optimal solution $\mathbf{e}_v^T = e^{j(u_h - \arg(\mathbf{h}'_{v,n'_s}))}$ and resulting in the following n_r th optimal vertical receive phase shift:

$$\gamma_{v(n_r)} = u_h - \arg(\mathbf{h}'_{v,n'_s(n_r)}), \quad n_r = 1, 2, \dots, N_r. \quad (8)$$

Similar to (P1.30), problem (P1.22) for \mathbf{e}_h^T is given by

$$\begin{aligned} \max_{\mathbf{e}_h} & \quad \left| \mathbf{e}_h^T \mathbf{h}'_{h,n'_s} \right|^2 \\ \text{s.t.} & \quad \left| \mathbf{e}_{h(n_r)} \right| = 1, \quad n_r = 1, \dots, N_r, \\ & \quad \arg(\mathbf{e}_h^T \mathbf{h}'_{h,n'_s}) = u_v, \end{aligned} \quad (\text{P1.31})$$

with the optimal solution $\mathbf{e}_h^T = e^{j(u_v - \arg(\mathbf{h}'_{h,n'_s}))}$ and the following n_r th optimal horizontal receive phase shift:

$$\gamma_{h(n_r)} = u_v - \arg(\mathbf{h}'_{h,n'_s(n_r)}), \quad n_r = 1, \dots, N_r, \quad (9)$$

where $u_v = \arg(\delta_{v,n'_s})$.

3) *Overall Algorithm for the Low-SNR Regime:* The algorithm for the low-SNR regime is summarized in Algorithm 2. The convergence of this algorithm is guaranteed by the fact that for each subproblem, the optimal solution is obtained, which ensures that the objective value of (P1.24) is monotonically non-decreasing over iterations.

Algorithm 2 Alternating Optimization Algorithm for the Low-SNR Regime

- 1: Set iteration $k = 0$ and initialize $\Theta_v^k = \mathbf{I}_{\Theta_v}$, $\Theta_h^k = \mathbf{I}_{\Theta_h}$, $\mathbf{E}_v^k = \mathbf{I}_{\mathbf{E}_v}$, and $\mathbf{E}_h^k = \mathbf{I}_{\mathbf{E}_h}$.
 - 2: Solve (P1.1) for strongest eigenchannel and denote the optimized precoding and combining vectors as $\mathbf{f}_{n_s}^k$ and $\mathbf{w}_{n_s}^{*k}$, respectively.
 - 3: **repeat**
 - 4: Given \mathbf{E}_v^k , \mathbf{E}_h^k , and Θ_h^k , calculate the optimal Θ_v^{k+1} using (6).
 - 5: Given Θ_v^{k+1} , calculate the optimal Θ_h^{k+1} using (7).
 - 6: Given Θ_v^{k+1} , Θ_h^{k+1} , and \mathbf{E}_h^k , calculate the optimal \mathbf{E}_v^{k+1} using (8).
 - 7: Given \mathbf{E}_v^{k+1} , calculate the optimal \mathbf{E}_h^{k+1} using (9).
 - 8: Given Θ_v^{k+1} , Θ_h^{k+1} , \mathbf{E}_v^{k+1} , and \mathbf{E}_h^{k+1} , calculate the optimal $\mathbf{f}_{n_s}^{k+1}$, $\mathbf{w}_{n_s}^{*k+1}$, and n_s^{k+1} by solving (P1.1) for strongest eigenchannel.
 - 9: Update $k = k + 1$.
 - 10: **until** the objective value of (P1.24) converges or the maximum number of iterations are completed.
-

B. High-SNR Regime and Rich Scattering Scenario

In a high-SNR regime and rich scattering environment, the optimal way to maximize the SE of a MIMO channel is to divide the total transmit power equally to all available eigenchannels [37]. Hence, problem (P1) can be approximated as [37]

$$\begin{aligned}
 & \max_{\Theta_v, \Theta_h, \mathbf{E}_v, \mathbf{E}_h} \sum_{n_s=1}^{N_s} \left| \mathbf{w}_{n_s}^* \left\{ \mathbf{E}_h \left(\mathbf{H}_{r,v}^H \Theta_v \mathbf{G} + \mathbf{H}_{d,v}^H \right) + \mathbf{E}_h \left(\mathbf{H}_{r,h}^H \Theta_h \mathbf{G} + \mathbf{H}_{d,h}^H \right) \right\} \mathbf{f}_{n_s} \right|^2 \\
 \text{s.t.} \quad & \Theta_p = \text{diag}(e^{-j\phi_{p,1}}, e^{-j\phi_{p,2}}, e^{-j\phi_{p,3}}, \dots, e^{-j\phi_{p,N}}), p \in \{v, h\}, \\
 & \mathbf{E}_p = \text{diag}(e^{-j\gamma_{p,1}}, e^{-j\gamma_{p,2}}, e^{-j\gamma_{p,3}}, \dots, e^{-j\gamma_{p,N_r}}), p \in \{v, h\}, \\
 & \|\mathbf{f}_{n_s}\|^2 = \frac{P_t}{N_s}, n_s = 1, 2, \dots, 2N_s.
 \end{aligned} \tag{P1.32}$$

Following the same method as in Section II, the SDR formulations for optimizing Θ_v , Θ_h , \mathbf{E}_v , and \mathbf{E}_h are given by

$$\begin{aligned}
 & \max_{\mathbf{L}_v} \xi_{\mathbf{L}_v} \\
 \text{s.t.} \quad & \mathbf{x}_{\mathbf{L}_v} = [(\text{trace}(\mathbf{O}_{v,1} \mathbf{L}_v) + |\eta_{v,1}|^2), \dots, (\text{trace}(\mathbf{O}_{v,n_s} \mathbf{L}_v) + |\eta_{v,n_s}|^2)] \\
 & \mathbf{L}_{v(n,n)} = 1, \quad n = 1, \dots, N + 1, \\
 & \mathbf{L}_v \succeq 0, \\
 & \text{sum}(\mathbf{x}_{\mathbf{L}_v}) \geq \lambda'_{\mathbf{L}_v} + \xi_{\mathbf{L}_v},
 \end{aligned} \tag{P1.33}$$

$$\begin{aligned}
& \max_{\mathbf{L}_h} \xi_{\mathbf{L}_h} \\
\text{s.t.} \quad & \mathbf{x}_{\mathbf{L}_h} = [(\text{trace}(\mathbf{O}_{h,1}\mathbf{L}_h) + |\eta_{h,1}|^2), \dots, (\text{trace}(\mathbf{O}_{h,n_s}\mathbf{L}_h) + |\eta_{h,n_s}|^2)] \\
& \mathbf{L}_{h(n,n)} = 1, \quad n = 1, \dots, N+1, \\
& \mathbf{L}_h \succeq 0, \\
& \text{sum}(\mathbf{x}_{\mathbf{L}_h}) \geq \lambda'_{\mathbf{L}_h} + \xi_{\mathbf{L}_h},
\end{aligned} \tag{P1.34}$$

$$\begin{aligned}
& \max_{\mathbf{\Xi}_v} \xi_{\mathbf{\Xi}_v} \\
\text{s.t.} \quad & \mathbf{x}_{\mathbf{\Xi}_v} = [(\text{trace}(\mathbf{S}_1^v\mathbf{\Xi}_v) + |\gamma_h|^2), \dots, (\text{trace}(\mathbf{S}_{n_s}^v\mathbf{\Xi}_v) + |\gamma_h|^2)] \\
& \mathbf{\Xi}_{v(n_r,n_r)} = 1, \quad n = 1, \dots, N_r+1, \\
& \mathbf{\Xi}_v \succeq 0, \\
& \text{sum}(\mathbf{x}_{\mathbf{\Xi}_v}) \geq \lambda'_{\mathbf{\Xi}_v} + \xi_{\mathbf{\Xi}_v},
\end{aligned} \tag{P1.35}$$

and

$$\begin{aligned}
& \max_{\mathbf{\Xi}_h} \xi_{\mathbf{\Xi}_h} \\
\text{s.t.} \quad & \mathbf{x}_{\mathbf{\Xi}_h} = [(\text{trace}(\mathbf{S}_1^h\mathbf{\Xi}_h) + |\gamma_v|^2), \dots, (\text{trace}(\mathbf{S}_{n_s}^h\mathbf{\Xi}_h) + |\gamma_v|^2)] \\
& \mathbf{\Xi}_{h(n_r,n_r)} = 1, \quad n = 1, \dots, N_r+1, \\
& \mathbf{\Xi}_h \succeq 0 \\
& \text{sum}(\mathbf{x}_{\mathbf{\Xi}_h}) \geq \lambda'_{\mathbf{\Xi}_h} + \xi_{\mathbf{\Xi}_h},
\end{aligned} \tag{P1.36}$$

respectively. The AO algorithm based on these formulations requires a lower computational cost than that of the AO in Section II for the following reasons: 1) There is no need to adopt the water-filling method in each AO iteration. 2) Solving problems based on $\text{sum}(\mathbf{x})$ is computationally less expensive than those based on $\text{GM}(\mathbf{x})$ [38]. Furthermore, in the high-SNR regime, the expressions for \mathbf{x} in (P1.33), (P1.34), (P1.35), and (P1.36) are simpler than those in Section II. The overall algorithm is summarized in Algorithm 3.

If the environment is not favorable for Algorithm 3, the water-filling power allocation method in Algorithm 3 can result in better performance than Algorithm 3 with equal power distribution. The performance analysis of Algorithm 3 with optimal power allocation is also presented in Section V-B.

Algorithm 3 Alternating Optimization Algorithm for High SNR regime

- 1: Set iteration $k = 0$ and initialize $\Theta_v^k = \mathbf{I}_{\Theta_v}$, $\Theta_h^k = \mathbf{I}_{\Theta_h}$, $\mathbf{E}_v^k = \mathbf{I}_{\mathbf{E}_v}$, $\mathbf{E}_h^k = \mathbf{I}_{\mathbf{E}_h}$, and $\xi_{\Xi_h}^k = 0$.
 - 2: Solve (P1.1) using the SVD, divide the total transmit power equally among the available eigenchannels, and denote the optimized \mathbf{W} , \mathbf{F} , and N_s as \mathbf{W}^k , \mathbf{F}^k , and N_s^k , respectively.
 - 3: **repeat**
 - 4: Given \mathbf{E}_v^k , \mathbf{E}_h^k , and Θ_h^k , put $\lambda'_{\mathbf{L}_v} = \xi_{\Xi_h}^k$, solve (P1.33), retrieve optimal Θ_v^{k+1} from \mathbf{L}_v using Gaussian randomization, and denote the maximized objective value as $\xi_{\mathbf{L}_v}^k$.
 - 5: Given Θ_v^{k+1} , put $\lambda'_{\mathbf{L}_h} = \xi_{\mathbf{L}_v}^k$, solve (P1.34), retrieve optimal Θ_h^{k+1} from \mathbf{L}_h using Gaussian randomization, and denote the maximized objective value as $\xi_{\mathbf{L}_h}^k$.
 - 6: Given Θ_v^{k+1} , Θ_h^{k+1} , and \mathbf{E}_h^k , put $\lambda'_{\Xi_v} = \xi_{\mathbf{L}_h}^k$, solve (P1.35), retrieve optimal \mathbf{E}_v^{k+1} from Ξ_v using Gaussian randomization, and denote the maximized objective value as $\xi_{\Xi_v}^k$.
 - 7: Given \mathbf{E}_v^{k+1} , put $\lambda'_{\Xi_h} = \xi_{\Xi_v}^k$, solve (P1.36), retrieve optimal \mathbf{E}_h^{k+1} from Ξ_h using Gaussian randomization, and denote the maximized objective value as $\xi_{\Xi_h}^{k+1}$.
 - 8: Given Θ_v^{k+1} , Θ_h^{k+1} , \mathbf{E}_h^{k+1} , and \mathbf{E}_v^{k+1} , solve (P1.1) using the SVD, divide the total transmit power equally among the available eigenchannels, and denote the optimized \mathbf{W} , \mathbf{F} , and N_s as \mathbf{W}^{k+1} , \mathbf{F}^{k+1} , and N_s^{k+1} , respectively.
 - 9: Update $k = k + 1$.
 - 10: **until** the objective value of (P1.32) converges or the maximum number of iterations are completed.
-

V. SIMULATION RESULTS

A. Simulation Setup

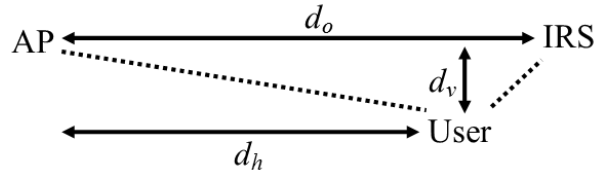


Fig. 2. Simulation setup.

In this section, we provide the numerical analysis results to determine the performance of the proposed algorithms. The simulation setup, which is widely used for research, is illustrated in Fig. 2 [6], [7], [40]. Owing to the moving capability of the user, we consider Rayleigh fading

for the AP-user and IRS-user links, whereas the AP-IRS link is modeled by Rician fading [41]. Specifically, the AP-IRS channel is given by

$$\mathbf{G}_p = \sqrt{\frac{\chi}{1+\chi}} \mathbf{G}_p^{LoS} + \sqrt{\frac{1}{1+\chi}} \mathbf{G}_p^{NLoS}, \quad p \in \{v, h\}, \quad (10)$$

where \mathbf{G}_p^{LoS} and \mathbf{G}_p^{NLoS} represent LoS and non-LoS (i.e., Rayleigh) components of \mathbf{G}_p , respectively, and χ denotes the Rician factor. The variation in the value of χ determines the dominant type of AP-IRS link, i.e., LoS or Rayleigh. The AP-IRS distance (d_o) and IRS-user vertical distance (d_v) are fixed at 40 m and 2 m, respectively. The AP-user horizontal distance, denoted by d_h , is varied to observe the change in performance. After setting d_h , d_o , and d_v , we can calculate the direct distances between the AP, IRS, and the user. To determine the path loss for each link, we use

$$PL(\text{dB}) = C_o + 10a \log\left(\frac{d}{D_o}\right), \quad (11)$$

where a is the path loss exponent, C_o is the path loss (dB) at a reference distance of D_o , and d is the distance between links. According to [6], we set $D_o = 1$ m, $C_o = 30$ dB, $P_t = 40$ dBm, $\sigma^2 = -94$ dBm, and $N_t = N_r = 4$ unless otherwise stated. Furthermore, we assume $a = 2.2, 3.5$, and 2.5 for the AP-IRS, AP-User, and IRS-User links, respectively, [6]. All simulation results are averaged over 100 channel realizations and performed using MATLAB R2022a on an AMD Ryzen R7-5800H CPU @3.20GHz with 16 GB of RAM.

B. Simulation Results

First, we set $N = 50$, $d_h = 38$ meters, and $\chi = -20$ dB, and plot the convergence behavior and show the time complexity of Algorithm 1 in Fig. 3. Specifically, in Fig. 3, Algorithm 1 is simulated based on the following three formulations:

- 1) AO based on (P1.10) formulation: Algorithm 1 solves (P1.10) and it can be observed that it requires a significantly higher computational cost than the other two formulations because of $\text{logsum}(\mathbf{x})$ expressions [39].
- 2) AO based on (P1.12) formulation: Algorithm 1 solves (P1.12) and it can be observed that it takes more iterations than Case 2 because there is no objective function.
- 3) AO based on (P1.13) formulation: Algorithm 1 solves (P1.13), where a slack variable and $\text{GM}(\mathbf{x})$ serve as an alternative to the objective function and $\text{logsum}(\mathbf{x})$, respectively. It can be observed in Fig. 3 that Algorithm 1, based on this formulation, requires the lowest computational cost.

Furthermore, in Fig. 3, it can be seen that the Algorithm 1 provides 65.6 % increase in SE compared to that of the initial point and the first iteration achieves 83.3 % of the final converged value.

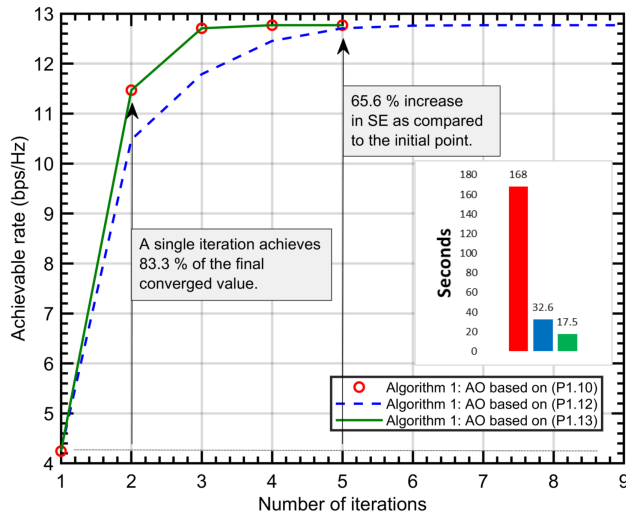


Fig. 3. Convergence behavior of Algorithm 1 with $N = 50$.

In Table I, we present the computational complexity of Algorithms 1, 2, and 3 in terms of the average CPU running time. It can be inferred that Algorithms 2 and 3 achieve significant reductions in computational complexity compared with Algorithm 1. Specifically, for $N = 50$ and 16×16 MIMO, Algorithms 1, 2, and 3 take 19.57 s, 10.02 ms, and 4.19 s, respectively. Furthermore, in Table I, it can be noted that because of the closed-form solutions, Algorithm 2 is significantly faster; in other words, it requires only several milliseconds for convergence.

TABLE I
AVERAGE CPU RUNNING TIME FOR ALGORITHMS 1, 2, AND 3.

Algorithm	$N = 10$	$N = 30$	$N = 50$	$N = 10$	$N = 30$	$N = 50$
	4×4 MIMO			16×16 MIMO		
Algorithm 1	1.83 s	3.17 s	17.51 s	2.96 s	5.02 s	19.57 s
Algorithm 2	5.82 ms	7.11 ms	9.40 ms	7.13 ms	8.27 ms	10.02 ms
Algorithm 3	1.12 s	2.05 s	6.61 s	1.61 s	2.22 s	4.19 s

Next, in Figs. 4 and 5, we plot the SE performance versus the number of reflecting elements for $\chi = 20$ dB and -20 dB, respectively. The comparison schemes are as follows.

- 1) Algorithm 1: In Figs. 4 and 5, it can be observed that Algorithm 1, i.e., SDR based AO, achieves the best performance in both scenarios, i.e., Rayleigh and LoS.
- 2) Without DP-IRS: There is no IRS and the precoder \mathbf{F} and combiner \mathbf{W} are optimized based on SVD and the water-filling technique. It is observed that without IRS, the user achieves the worst SE performance.
- 3) Random DP-IRS and receive phase shifters: We consider random phases for both DP-IRS and receive phase shifters. In Figs. 4 and 5, it can be observed that the random operations result in the significantly lower SE performance as compared to that of Algorithm 1.
- 4) Random DP-IRS and optimized receive phase shifters: To demonstrate the impact of optimal receive phase shifters on the SE performance, in Algorithm 1, we consider random DP-IRS phases and optimal receive phase shifts. It can be observed that even if the DP-IRS operations are random, optimizing only receive phase shifters improves SE performance.
- 5) Algorithm 2: We solve the problem (P1) using Algorithm 2, which is designed for the low-SNR regime and/or LoS scenarios. It can be observed that for $\chi = 20$ dB in Fig. 4, Algorithm 2 achieves almost the same performance as Algorithm 1 with significantly lower computational cost, as presented in Table I. Furthermore, in Fig. 5, for $\chi = -20$ dB, i.e., Rayleigh fading, Algorithm 2 still performs very close to Algorithm 2 when N is small. However, as N increases, the performance difference between Algorithms 1 and 2 becomes larger because large values of N result in high SNRs.
- 6) Algorithm 3: We consider Algorithm 3, which is designed for high-SNR and rich-scattering environments. This algorithm exhibits optimal performance only when the powers of all eigenchannels are equally strong [37]. In Fig. 5, it can be observed that as N increases, i.e., varying from the low-SNR regime to the high-SNR regime, the SE performance of Algorithm 3 gets better than that of Algorithm 2. However, in Fig. 4, where the dominant effective channel is LoS, Algorithm 3 results in poor performance.
- 7) Algorithm 3 with optimal power distribution: We consider algorithm 3 with optimal power distribution. It can be observed in Figs. 4 and 5 that Algorithm 3 with optimal power distribution achieves a significantly better performance. Specifically, in Fig. 5, where $\chi = -20$ dB, it performs close to Algorithm 1.

Next, in Figs. 6 and 7, we plot the SE performance versus the total transmit power for $\chi = 20$ dB and -20 dB, respectively. Again, Algorithm 1 achieves the best performance in both

the figures. In general, similar relative performance behaviors are observed, as illustrated in Figs. 4 and 5.

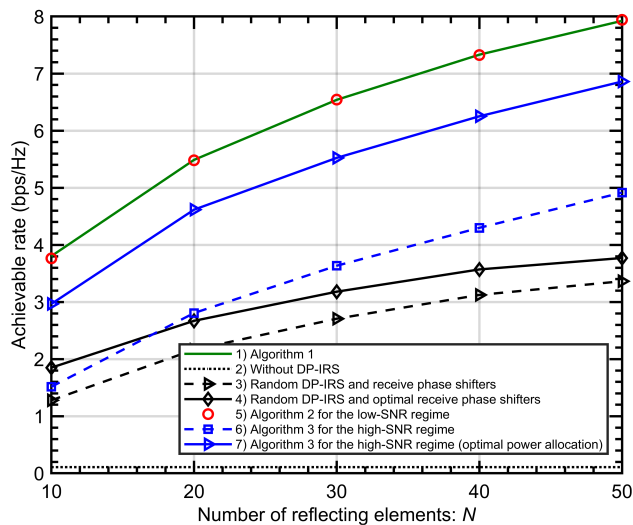


Fig. 4. Achievable rate versus the number of reflecting elements for $\chi = 20$ dB.

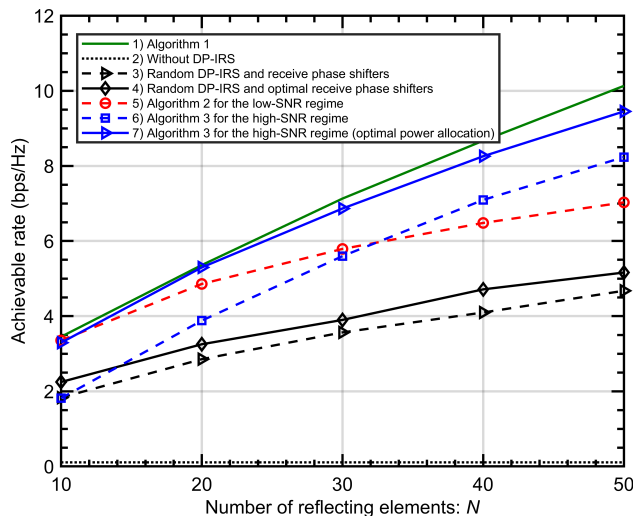


Fig. 5. Achievable rate versus the number of reflecting elements for $\chi = -20$ dB.

In Fig. 8, we demonstrate the SE performance versus the Rician factor χ . Specifically, for $N = 50$ and $d_h = 38$ m, we vary χ from -10 dB to 10 dB, i.e., from Rayleigh to LoS. In Fig. 8, it can be observed that as the channel changes from Rayleigh to LoS, the SE performance of Algorithm 2 improves. The opposite behavior can be observed in Algorithm 3. Overall, Algorithm 1 maintains the best SE performance for all values of χ .

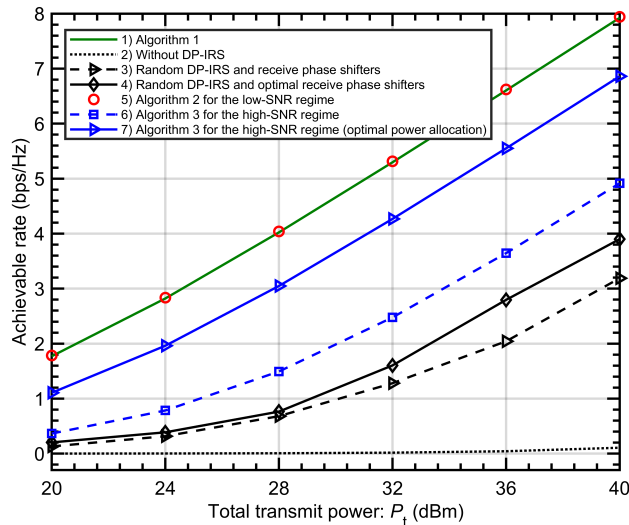


Fig. 6. Achievable rate versus the total transmit power for $\chi = 20$ dB.

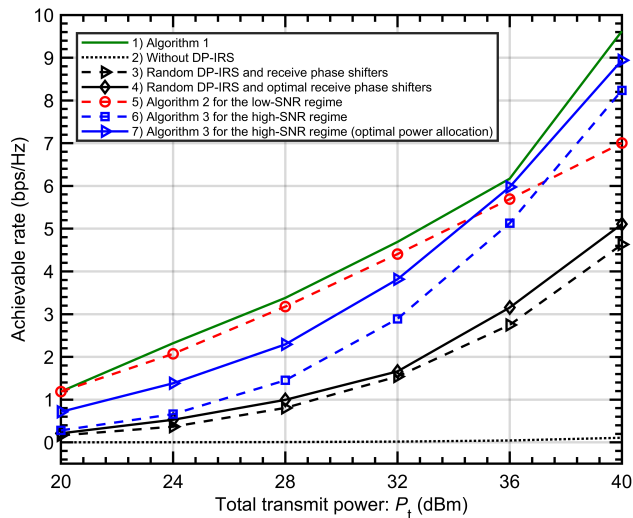


Fig. 7. Achievable rate versus the total transmit power for $\chi = -20$ dB.

Next, in Figs. 9 and 10, we move the user from the AP to the IRS and plot the resulting SE performance for $\chi = 20$ dB and -20 dB, respectively. Specifically, for $N = 50$, we alter d_h from 20 m to 40 m. In Figs. 9 and 10, when the user is near the AP and far from the DP-IRS, i.e., $d_h < 32$ m, the SE performance is mainly determined by the AP-user direct link. Hence, it can be observed that schemes employing the optimal power allocation method, i.e., Schemes 1, 2, 3, 4, and 7, achieve similar SE performance. In contrast, the SE performance is lower in the other schemes, i.e., Schemes 5 and 6, where we allocate all power to a single data stream

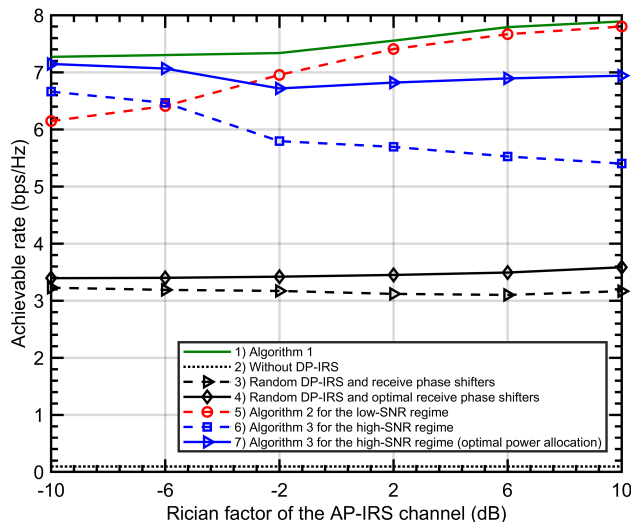


Fig. 8. Achievable rate versus the Rician factor of AP-IRS link.

or divide equally to all available data streams. However, when the user is very close to the AP, i.e., $d_h < 23\text{m}$, the SNR becomes high; hence, for $d_h < 23\text{m}$, it is evident in Figs. 9 and 10 that Algorithm 3 has improved performance. When the user is located near the DP-IRS, i.e., $d_h > 36\text{m}$, we observe similar performance behaviors, as illustrated in Figs. 4 and 5.

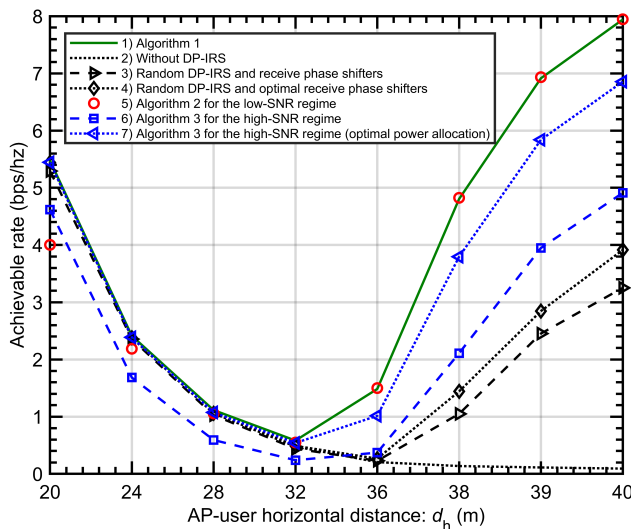


Fig. 9. Achievable rate versus the AP-user horizontal distance for $\chi = 20\text{ dB}$.

Finally, in Figs. 12 and 13 for $\chi = 20\text{ dB}$ and -20 dB , respectively, we consider the different numbers of transmit/receive antennas and plot the SE performance of S-IRS and DP-IRS versus

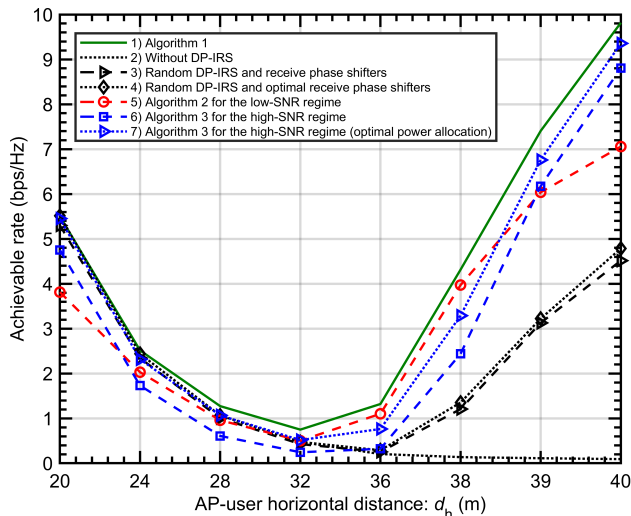


Fig. 10. Achievable rate versus the AP-user horizontal distance for $\chi = -20$ dB.

the number of reflecting elements. In particular, we consider 4×4 , 8×8 , and 16×16 MIMO configurations.

The system model for the S-IRS-assisted MIMO network is shown in Fig. 11, where each reflecting element of S-IRS introduces phase and amplitude changes in the reflected signals. The operation of a single reflecting element is represented by $\omega e^{-j\phi}$, where ω and ϕ denote the induced amplitude and phase changes, respectively. Similar to our proposed work, we assume full-reflection for each element of the S-IRS, which is achieved by setting $\omega = 1$ for all reflecting elements. For this comparison, we derive a formulation equivalent to (P1.13) for S-IRS phases and devise an AO algorithm that optimizes the IRS phases and precoder/combiner alternatively until convergence is reached. Furthermore, for a fair comparison, we normalize the operation (1) of each reflecting element of the DP-IRS by a factor of $\frac{1}{\sqrt{2}}$, that is, $\frac{1}{\sqrt{2}}\Psi$.

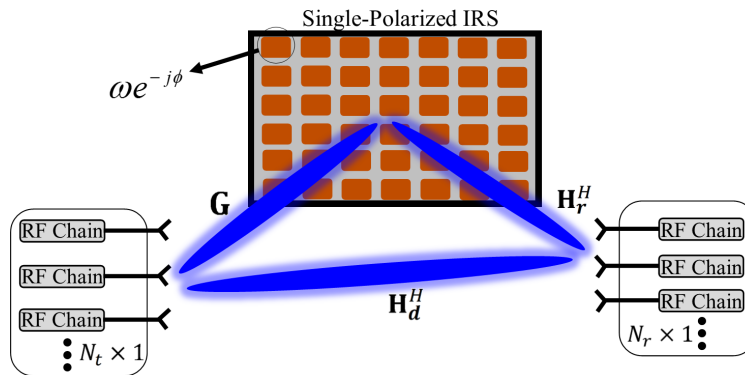


Fig. 11. System model for the S-IRS-assisted MIMO system.

Overall, in Figs. 12 and 13, it can be observed that increasing N , N_t , and N_r improves the SE performance for both S-IRS and DP-IRS. However, because of the PM gains, DP-IRS performs substantially better than S-IRS. Specifically, in Fig. 13, for $\chi = -20$ dB, i.e., Rayleigh fading, more reflecting elements or antennas in the rich scattered environment help DP-IRS to better utilize its PM and PD capabilities, which result in a significantly better SE performance than that of S-IRS. In Fig. 12, where $\chi = 20$ dB, i.e., LoS channel, increasing N does not help much in the increase of performance difference between S-IRS and DP-IRS. This is because as long as the dominant channel is LoS, increasing N does not help much to increase the data streams.

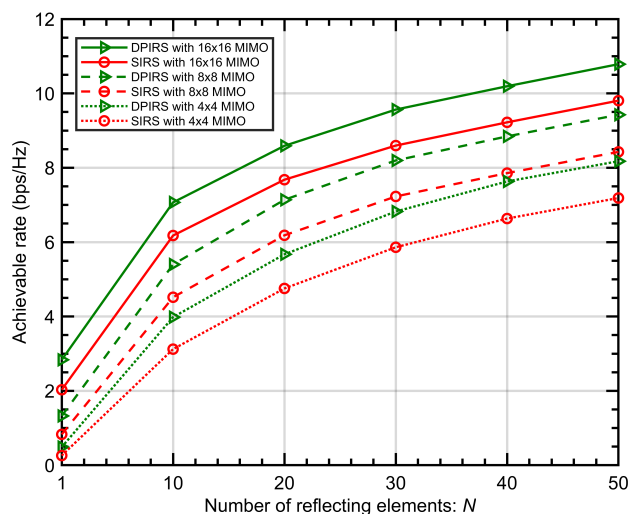


Fig. 12. Achievable rate of DP-IRS and S-IRS versus the number of reflecting elements for various MIMO configurations ($\chi = 20$ dB).

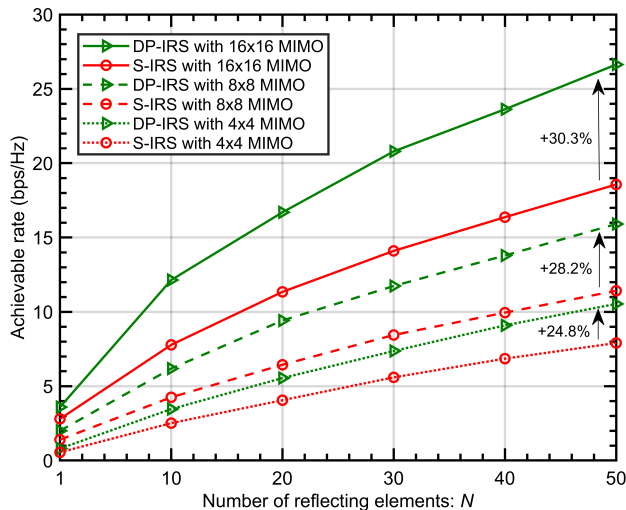


Fig. 13. Achievable rate of DP-IRS and S-IRS versus the number of reflecting elements for various MIMO configurations ($\chi = -20$ dB).

VI. CONCLUSION

To maximize the SE performance of the DP-IRS-assisted MIMO network, we optimize the operations of the reflecting elements at the DP-IRS, precoder/combiner at the transmitter/receiver, and vertical/horizontal phase shifters at the DP antennas. To solve the formulated capacity maximization problem, we propose an SDR-based AO algorithm, which operates by addressing several subproblems alternately until the SE performance converges. The convex formulations of the sub-problems are shaped, such that the algorithm is guaranteed to converge. Furthermore, considering the low/high SNR regimes, we provide two AO algorithms that are computationally efficient than the first approach. Specifically, for the low-SNR regime, we derive closed-form solutions. We provide extensive numerical results for the SE performance of the DP-IRS by varying the number of reflecting elements, total transmit power, user locations, and type of channels. The numerical results show that the proposed algorithms outperform various benchmark schemes. Specifically, Algorithm 1 achieves a 65.6 % increase in SE performance compared with random operations and, on average, needs five iterations for convergence. Moreover, a single iteration of Algorithm 1 achieves 83.3 % of the final converged performance. For the low-SNR regime and/or LoS dominant channel, Algorithm 2 achieves almost the same performance as Algorithm 1 but with a substantially lower computational cost. Specifically, in terms of average CPU running time, for $N = 50$ and $N_t = N_r = 16$, Algorithms 1 and 2 take 19.57 s and 10.02 ms, respectively. We also provide the SE performances of S-IRS and compare them with

those of DP-IRS. The numerical results show that for $N = 50$ and Rayleigh fading, DP-IRS achieves 24.8 %, 28.2 %, and 30.3 % improvements in SE for 4×4 , 8×8 , and 16×16 MIMO, respectively, compared to the S-IRS. It is noted that the operation of a single reflecting element of the DP-IRS is computationally more expensive than that of a single element of the S-IRS. However, because of the inherent capabilities of DP waves in DP-IRS, we believe that the DP-IRS has much potential over the S-IRS. Correspondingly, an interesting future work could be to investigate the design and performance of the extension of this work to multi-users cases with more practical considerations such as hardware-constrained reflection at DP-IRS, polarization power leakage, imperfect/partial channel state information, etc.

REFERENCES

- [1] J. Y. Dai, W. Tang, M. Z. Chen, C. H. Chan, Q. Cheng, S. Jin, and T. J. Cui, "Wireless Communication Based on Information Metasurfaces," *IEEE Trans. Microw. Theory Techn.*, vol. 69, no. 3, pp. 1493–1510, 2021.
- [2] Ö. Özdoğan, E. Björnson, and E. G. Larsson, "Intelligent reflecting surfaces: Physics, propagation, and pathloss modeling," *IEEE Wireless Commun. Lett.*, vol. 9, no. 5, pp. 581–585, 2019.
- [3] S. Abeywickrama, R. Zhang, Q. Wu, and C. Yuen, "Intelligent reflecting surface: Practical phase shift model and beamforming optimization," *IEEE Trans. Commun.*, vol. 68, no. 9, pp. 5849–5863, 2020.
- [4] T. J. Cui, M. Q. Qi, X. Wan, J. Zhao, and Q. Cheng, "Coding metamaterials, digital metamaterials and programmable metamaterials," *Light: Sci. & Appl.*, vol. 3, no. 10, pp. e218–e218, 2014.
- [5] S. Gong, X. Lu, D. T. Hoang, D. Niyato, L. Shu, D. I. Kim, and Y.-C. Liang, "Toward smart wireless communications via intelligent reflecting surfaces: A contemporary survey," *IEEE Commun. Surv. Tutor.*, vol. 22, no. 4, pp. 2283–2314, 2020.
- [6] Q. Wu and R. Zhang, "Intelligent reflecting surface enhanced wireless network via joint active and passive beamforming," *IEEE Trans. Wireless Commun.*, vol. 18, no. 11, pp. 5394–5409, 2019.
- [7] —, "Beamforming optimization for wireless network aided by intelligent reflecting surface with discrete phase shifts," *IEEE Trans. on Commun.*, vol. 68, no. 3, pp. 1838–1851, 2019.
- [8] J. Chen, Y.-C. Liang, Y. Pei, and H. Guo, "Intelligent reflecting surface: A programmable wireless environment for physical layer security," *IEEE Access*, vol. 7, pp. 82 599–82 612, 2019.
- [9] M. Cui, G. Zhang, and R. Zhang, "Secure wireless communication via intelligent reflecting surface," *IEEE Wireless Commun. Lett.*, vol. 8, no. 5, pp. 1410–1414, 2019.
- [10] L. Dong and H.-M. Wang, "Secure MIMO transmission via intelligent reflecting surface," *IEEE Wireless Commun. Lett.*, vol. 9, no. 6, pp. 787–790, 2020.
- [11] H. Yang, Z. Xiong, J. Zhao, D. Niyato, L. Xiao, and Q. Wu, "Deep reinforcement learning-based intelligent reflecting surface for secure wireless communications," *IEEE Trans. Wireless Commun.*, vol. 20, no. 1, pp. 375–388, 2020.
- [12] K. Feng, X. Li, Y. Han, S. Jin, and Y. Chen, "Physical layer security enhancement exploiting intelligent reflecting surface," *IEEE Commun. Lett.*, vol. 25, no. 3, pp. 734–738, 2020.
- [13] Y. Jia, C. Ye, and Y. Cui, "Analysis and optimization of an intelligent reflecting surface-assisted system with interference," *IEEE Trans. Wireless Commun.*, vol. 19, no. 12, pp. 8068–8082, 2020.
- [14] M. Jiang, Y. Li, G. Zhang, and M. Cui, "Achievable rate region maximization in intelligent reflecting surfaces-assisted interference channel," *IEEE Trans. Veh. Technol.*, vol. 70, no. 12, pp. 13 406–13 412, 2021.

- [15] C. Pan, H. Ren, K. Wang, M. ElKashlan, A. Nallanathan, J. Wang, and L. Hanzo, "Intelligent reflecting surface aided MIMO broadcasting for simultaneous wireless information and power transfer," *IEEE J. Sel. Areas Commun.*, vol. 38, no. 8, pp. 1719–1734, 2020.
- [16] F. El Bouanani, S. Muhaidat, P. C. Sofotasios, O. A. Dobre, and O. S. Badarneh, "Performance analysis of intelligent reflecting surface aided wireless networks with wireless power transfer," *IEEE Commun. Lett.*, vol. 25, no. 3, pp. 793–797, 2020.
- [17] S. Lin, B. Zheng, G. C. Alexandropoulos, M. Wen, M. Di Renzo, and F. Chen, "Reconfigurable intelligent surfaces with reflection pattern modulation: Beamforming design and performance analysis," *IEEE Trans. Wireless Commun.*, vol. 20, no. 2, pp. 741–754, 2020.
- [18] M. Munawar and K. Lee, "Low-Complexity Adaptive Selection Beamforming for IRS-Assisted Single-User Wireless Networks," *IEEE Trans. Veh. Technol.*, vol. 72, no. 4, pp. 5458–5462, 2023.
- [19] B. Zheng, C. You, W. Mei, and R. Zhang, "A survey on channel estimation and practical passive beamforming design for intelligent reflecting surface aided wireless communications," *IEEE Commun. Surv. Tutor.*, vol. 24, no. 2, pp. 1035–1071, 2022.
- [20] Z. Wang, L. Liu, and S. Cui, "Channel estimation for intelligent reflecting surface assisted multiuser communications: Framework, algorithms, and analysis," *IEEE Trans. Wireless Commun.*, vol. 19, no. 10, pp. 6607–6620, 2020.
- [21] T. Jiang, H. V. Cheng, and W. Yu, "Learning to reflect and to beamform for intelligent reflecting surface with implicit channel estimation," *IEEE J. Sel. Areas Commun.*, vol. 39, no. 7, pp. 1931–1945, 2021.
- [22] R. G. Vaughan, "Polarization diversity in mobile communications," *IEEE Trans. Veh. Technol.*, vol. 39, no. 3, pp. 177–186, 1990.
- [23] W. Lee and Y. Yeh, "Polarization diversity system for mobile radio," *IEEE Trans. Commun.*, vol. 20, no. 5, pp. 912–923, 1972.
- [24] L. Deng, J. Deng, Z. Guan, J. Tao, Y. Chen, Y. Yang, D. Zhang, J. Tang, Z. Li, Z. Li *et al.*, "Malus-metasurface-assisted polarization multiplexing," *Light: Sci. Appl.*, vol. 9, no. 1, pp. 1–9, 2020.
- [25] B. Krongold, T. Pfau, N. Kaneda, and S. C. J. Lee, "Comparison between PS-QPSK and PDM-QPSK with equal rate and bandwidth," *IEEE Photon. Technol. Lett.*, vol. 24, no. 3, pp. 203–205, 2011.
- [26] A. S. de Sena, P. H. Nardelli, D. B. da Costa, F. R. M. Lima, L. Yang, P. Popovski, Z. Ding, and C. B. Papadias, "IRS-assisted massive MIMO-NOMA networks: Exploiting wave polarization," *IEEE Trans. Wirel. Commun.*, vol. 20, no. 11, pp. 7166–7183, 2021.
- [27] X. Chen, J. C. Ke, W. Tang, M. Z. Chen, J. Y. Dai, E. Basar, S. Jin, Q. Cheng, and T. J. Cui, "Design and implementation of MIMO transmission based on dual-polarized reconfigurable intelligent surface," *IEEE Wireless Commun. Lett.*, vol. 10, no. 10, pp. 2155–2159, 2021.
- [28] J. Shu, H. Peng, Y. Zhang, and J. Mao, "A dual polarized pattern reconfigurable antenna array using liquid crystal phase shifter," in *Proc. Int. Symp. Antennas Propag. (ISAP)*, 2018, pp. 1–2.
- [29] H. Arai, K. Abe, N. Takemura, and T. Mitsui, "Dual-polarized switched beam antenna with variable phase shifter," in *Proc. Int. Workshop on Antenna Technol. (iWAT)*, 2013, pp. 19–22.
- [30] E. Björnson, Ö. Özdogan, and E. G. Larsson, "Intelligent reflecting surface versus decode-and-forward: How large surfaces are needed to beat relaying?" *IEEE Wireless Commun. Lett.*, vol. 9, no. 2, pp. 244–248, 2019.
- [31] S. Zhang and R. Zhang, "Capacity characterization for intelligent reflecting surface aided MIMO communication," *IEEE J. Sel. Areas Commun.*, vol. 38, no. 8, pp. 1823–1838, 2020.
- [32] E. E. Bahingayi and K. Lee, "Low-Complexity Beamforming Algorithms for IRS-Aided Single-User Massive MIMO mmwave Systems," *IEEE Trans. Wireless Commun.*, vol. 21, no. 11, pp. 9200–9211, 2022.

- [33] S. Sun, W. Jiang, S. Gong, and T. Hong, "Reconfigurable linear-to-linear polarization conversion metasurface based on PIN diodes," *IEEE Antennas Wirel. Propag. Lett.*, vol. 17, no. 9, pp. 1722–1726, 2018.
- [34] J. Wang, R. Yang, R. Ma, J. Tian, and W. Zhang, "Reconfigurable multifunctional metasurface for broadband polarization conversion and perfect absorption," *IEEE Access*, vol. 8, pp. 105 815–105 823, 2020.
- [35] H. F. Ma, G. Z. Wang, G. S. Kong, and T. J. Cui, "Independent controls of differently-polarized reflected waves by anisotropic metasurfaces," *Sci. Rep.*, vol. 5, no. 1, p. 9605, 2015.
- [36] B. Clerckx and C. Oestges, *MIMO Wireless Networks: Channels, Techniques and Standards for Multi-Antenna, Multi-User and Multi-Cell Systems*, New York, NY, USA:Academic, 2013.
- [37] D. Tse and P. Viswanath, *Fundamentals of wireless communication*, Cambridge, U.K.:Cambridge Univ. Press, 2005.
- [38] M. Grant and S. Boyd, "CVX: Matlab Software for Disciplined Convex Programming," [online] Available:<http://cvxr.com/cvx>, [online] Available: <http://cvxr.com/cvx>.
- [39] —, "CVX: Advanced topics," [online] Available:<http://web.cvxr.com/cvx/beta/doc/advanced.html>.
- [40] Q. Wu and R. Zhang, "Intelligent reflecting surface enhanced wireless network: Joint active and passive beamforming design," in *Proc. IEEE Global Commun. Conf. (GLOBECOM)*, 2018, pp. 1–6.
- [41] M. Viswanathan, *Wireless Communication Systems in MATLAB*. Independently Published, 2020, [online] Available:<https://www.gaussianwaves.com/wireless-communication-systems-in-matlab/>.